Project 2543 | September 2026

SJSU SAN JOSÉ STATE UNIVERSITY

MTI MINETA TRANSPORTATION INSTITUTE

Performance Evaluation of Fiber-Reinforced Hot Mix Asphalt Containing Reclaimed Asphalt Shingles

Hani Alzraiee, PhD
Shadi Saadeh, PhD
Adam Mansara
Ashraf Rahim, PhD
Aaditya Ojha

California State University Transportation Consortium

CAL POLY

MINETA TRANSPORTATION INSTITUTE

Founded in 1991, the Mineta Transportation Institute (MTI), an organized research and training unit in partnership with the Lucas College and Graduate School of Business at San José State University (SJSU), increases mobility for all by improving the safety, efficiency, accessibility, and convenience of our nation's transportation system. Through research, education, workforce development, and technology transfer, we help create a connected world. MTI leads the California State University Transportation Consortium (CSUTC) funded by the State of California through Senate Bill 1 and the Rail Resilience to Severe Weather: Training and Research Program (RR2SW) funded by the Federal Railroad Administration. MTI focuses on three primary responsibilities:

Research

MTI conducts multi-disciplinary research focused on surface transportation that contributes to effective decision making. Research areas include: active transportation; planning and policy; security and counterterrorism; sustainable transportation and land use; transit and passenger rail; transportation engineering; transportation finance; transportation technology; and workforce and labor. MTI research publications undergo expert peer review to ensure the quality of the research.

Education and Workforce Development

To ensure the efficient movement of people and goods, we must prepare the next generation of skilled transportation professionals who can lead a thriving, forward-thinking transportation industry for a more connected world. To help achieve this, MTI sponsors a suite of workforce development and education opportunities. The Institute supports educational programs offered by the Lucas Graduate School of Business: a Master of Science in Transportation Management, plus graduate certificates that include High-Speed and Intercity Rail Management and Transportation Security Management. These flexible programs offer live online classes so that working transportation professionals can pursue an advanced degree regardless of their location.

Information and Technology Transfer

MTI utilizes a diverse array of dissemination methods and media to ensure research results reach those responsible for managing change. These methods include publication, seminars, workshops, websites, social media, webinars, and other technology transfer mechanisms. Additionally, MTI promotes the availability of completed research to professional organizations and works to integrate the research findings into the graduate education program. MTI's extensive collection of transportation-related publications is integrated into San José State University's world-class Martin Luther King, Jr. Library.

Report 26-26

Performance Evaluation of Fiber-Reinforced Hot Mix Asphalt Containing Reclaimed Asphalt Shingles

Hani Alzraiee, PhD
Ashraf Rahim, PhD
Shadi Saadeh, PhD
Aaditya Ojha
Adam Mansara

September 2026

A publication of the
Mineta Transportation Institute
Created by Congress in 1991

College of Business
San José State University
San José, CA 95192-0219

Technical Report Documentation Page

1. Report No.
26-26

2. Government Accession No.

3. Recipient's Catalog No.

4. Title and Subtitle
Performance Evaluation of Fiber Reinforced Hot Mix Asphalt Containing Reclaimed Asphalt Shingles

5. Report Date
September 2026

6. Performing Organization Code

7. Authors
Hani Alzraiee, PhD
Ashraf Rahim, PhD
Shadi Saadeh, PhD
Aaditya Ojha
Adam Mansara

8. Performing Organization Report
CA-MTI-2543

9. Performing Organization Name and Address
Mineta Transportation Institute
College of Business
San José State University
San José, CA 95192-0219

10. Work Unit No.

11. Contract or Grant No.
SB1-SJAUX_2023-26

12. Sponsoring Agency Name and Address
State of California SB1 2017/2018
Trustees of the California State University
Sponsored Programs Administration
401 Golden Shore, 5th Floor
Long Beach, CA 90802

13. Type of Report and Period Covered

14. Sponsoring Agency Code

15. Supplemental Notes
10.31979/mti.2026.2543

16. Abstract
Reclaimed asphalt shingles (RAS) offer a promising avenue for increasing recycled content in hot mix asphalt, but the aged, stiff binder they contribute tends to reduce cracking resistance, particularly at intermediate temperatures. This study investigated whether polymer fiber reinforcement can offset that brittleness while preserving rutting and moisture performance in mixtures containing both reclaimed asphalt pavement (RAP) and RAS. Fourteen asphalt mixtures were designed using a base blend of 25% RAP combined with RAS at either 3% or 5% by total mix weight. Two commercially available polymer fiber types, designated Fiber A and Fiber B, were added at dosages of 0.05%, 0.10%, and 0.15% by total weight. All mixtures were evaluated for rutting resistance and moisture susceptibility using the Hamburg Wheel Tracking test and for intermediate-temperature cracking resistance using the IDEAL Cracking Test. Statistical comparisons were carried out using one-way ANOVA with Tukey adjusted pairwise contrasts against the control mix. Fiber addition did not compromise rutting performance and, in several cases, produced statistically significant reductions in rut depth. All mixtures satisfied the Hamburg moisture damage threshold. Cracking resistance improved substantially with fiber reinforcement, with Fiber B consistently outperforming Fiber A across both RAS levels. Statistically significant improvements in CTindex were observed most reliably at the 0.10% and 0.15% dosages of Fiber B. These results indicate that polymer fiber reinforcement can support higher recycled material usage in asphalt mixtures without sacrificing mechanical performance, offering a practical path toward more sustainable pavement design within a balanced mix design framework.

17. Key Words
Hot mix asphalt (HMA), reclaimed asphalt pavement (RAP), polymer fiber (PF), hamburg tracker (HT), and cracking tolerance index (CTI).

19. Security Classif. (of this report)
Unclassified

20. Security Classif. (of this page)
Unclassified

21. No. of Pages
76

22. Price

Form DOT F 1700.7 (8-72)

DOI: 10.31979/mti.2026.2543

Mineta Transportation Institute
College of Business
San José State University
San José, CA 95192-0219

Email: mineta-institute@sjsu.edu

transweb.sjsu.edu/research/2543

Acknowledgments

This study was funded by the Mineta Transportation Institute (MTI) at San José State University. The authors gratefully acknowledge MTI for its financial support and guidance throughout the research process. The authors also thank the California Department of Transportation (Caltrans) for its continued investment in sustainable pavement research and the laboratory staff at California State University, Long Beach and California Polytechnic State University for their assistance with specimen preparation and performance testing.

Contents

List of Figures

List of Tables

Executive Summary

Highway agencies in the United States face the challenge of maintaining aging pavement infrastructure while meeting environmental and sustainability goals. The increasing use of reclaimed asphalt pavement (RAP) and reclaimed asphalt shingles (RAS) in hot mix asphalt (HMA) represents a key strategy for reducing virgin material consumption, minimizing construction waste, and lowering greenhouse gas emissions. In California, Senate Bill 1 (SB1) investments of approximately $5.4 billion per year have further incentivized the adoption of durable, cost-effective, and sustainable pavement materials.

While RAS provides significant binder content and can replace a portion of virgin materials, its highly oxidized, stiff binder creates a well-documented tradeoff: Mixtures with higher RAS content exhibit improved rutting resistance but increased brittleness and susceptibility to cracking. This stiffness-induced rutting–cracking tradeoff has limited agency adoption of higher RAS levels, despite landfill diversion and cost-saving motivations. Polymer fiber reinforcement has shown promise in addressing these performance concerns in conventional and high-RAP asphalt mixtures, but limited research has examined the combined use of fibers and RAS.

This study evaluated dense-graded HMA mixtures containing 25% RAP with 3% and 5% RAS, reinforced with two para-aramid fiber types (Fiber A: wax-coated; Fiber B: liquid emulsion-treated) at dosages of 0.05%, 0.10%, and 0.15% by total mix weight. Performance testing aligned with the Balanced Mix Design (BMD) framework, using the Hamburg Wheel Tracking (HWT) test for rutting and moisture resistance and the IDEAL Cracking Test (IDEAL-CT) for intermediate-temperature cracking resistance.

Key findings include:

- Increasing RAS content from 3% to 5% in the control mixtures reduced rut depth from 3.66 mm to 2.87 mm at 15,000 wheel passes, confirming improved rutting resistance at higher RAS levels. However, the corresponding CTindex dropped from 55.42 to 21.04, confirming substantially reduced cracking tolerance and the expected rutting–cracking tradeoff.

- Fiber addition generally improved both rutting and cracking performance. In 5% RAS mixtures, Fiber A at 0.10% and 0.15% and Fiber B at 0.05% and 0.15% produced statistically significant reductions in rut depth. For cracking, Fiber B at 0.10% in 3% RAS mixtures was the only statistically significant improvement at the lower RAS level (CTindex = 119.79, more than double the control). In 5% RAS mixtures, Fiber A was significant at 0.15% (CTindex = 97.23) while Fiber B was significant at all dosages, with peak performance at 0.15% (CTindex = 106.90).

- All mixtures exhibited adequate moisture resistance with no stripping observed before 10,000 wheel passes under HWT testing, confirming that fiber incorporation and increased RAS content did not introduce moisture susceptibility.
- Fiber B consistently outperformed Fiber A in cracking resistance, attributed to its higher active para-aramid content (≥75% vs. ≥63%) and liquid emulsion treatment that promotes improved fiber dispersion and bonding within the asphalt mastic.
- These results demonstrate that properly engineered polymer fiber reinforcement can restore balanced performance in high RAP-RAS asphalt mixtures, supporting broader adoption of recycled materials under performance-based mix design frameworks. Future work should include field validation, extended aging protocols, and life-cycle cost analyses.

1. Introduction

Highway agencies in the United States are trying to maintain an aging pavement network while also meeting new environmental and climate goals. In California, Senate Bill 1 (SB1), known as the Road Repair and Accountability Act of 2017, invests about $5.4 billion per year to improve roads, freeways, and bridges, while supporting safety and transit projects (Caltrans, 2025). This major investment has pushed agencies to look for pavement materials that last longer, cost less to maintain, and reduce environmental impacts over their life cycle. Hot mix asphalt (HMA) is still the most widely used paving material in the United States, but traditional volumetric mix design is not always sufficient for today's traffic, climate conditions, and sustainability requirements.

One important sustainability strategy is using reclaimed asphalt pavement (RAP) and reclaimed asphalt shingles (RAS) in new asphalt mixtures. In 2022, asphalt producers in the United States used roughly 98.1 million tons of RAP and 1.4 million tons of RAS. This reuse saved about 5 million tons of asphalt binder and 93 million tons of virgin aggregates (Williams et al., 2024). These practices help reduce greenhouse gas emissions, conserve natural resources, and keep large amounts of waste out of landfills (National Asphalt Pavement Association [NAPA], 2016; Sias, 2024a). Research from NAPA has shown that well-designed mixtures with high binder replacement from RAP and RAS can reduce production energy by around 15 percent and lower emissions by 10 to 20 percent while still performing adequately in the field (NAPA, 2016).

RAS is especially attractive from a recycling standpoint. The United States generates an estimated 13.2 million tons of waste shingles every year, but only a small portion is typically recycled for pavement use (NAPA, 2019). California specifically produces large amounts of asphalt shingle waste, much of which ends up in landfills (San Diego County Department of Public Works [DPW], 2025). RAS contains a high amount of aged asphalt binder along with granules and mineral filler. This allows it to replace both virgin binder and aggregate (NAPA, 2019). However, the binder in RAS is extremely stiff. At higher replacement levels, it can make the mixture brittle and more prone to cracking if not managed carefully through design (Federal Highway Administration [FHWA], 2018; NAPA, 2016).

Although RAP/RAS mixtures generally improve rutting resistance through increased stiffness, moisture-induced damage can still cause stripping-related rutting, justifying the need for Hamburg Wheel Tracking testing. Field and laboratory studies show that mixtures with high RAP or RAS contents often have good rutting resistance but may have reduced cracking resistance compared with conventional HMA. This issue is especially noticeable in cold climates and under heavy traffic loading (FHWA, 2018; NAPA, 2016). Because of these concerns, many agencies limit the amount of RAS allowed in surface mixes or restrict its use entirely (FHWA, 2021; San Diego County DPW, 2025). At the same time, environmental policies and landfill diversion goals are encouraging agencies to consider higher recycled contents as long as mixtures can meet performance standards.

These challenges have encouraged a shift from a traditional volumetric mix design toward performance-based approaches such as Balanced Mix Design (BMD). BMD follows AASHTO PP 105 and requires the use of performance tests to evaluate both rutting and cracking characteristics under appropriate conditioning (NAPA, 2025). This approach allows engineers to design asphalt mixtures that balance performance rather than simply meeting volumetric criteria. For mixtures containing RAP or RAS, BMD has proven useful for determining the appropriate virgin binder grade, recycling level, and use of rejuvenators or modifiers to maintain performance (NAPA, 2016; NAPA, 2025). Alongside this movement, researchers and agencies are also exploring polymer and synthetic fibers to improve mixture durability. Fibers such as aramid, polypropylene, polyester, polyolefin, and glass can reinforce the asphalt mastic and help delay crack initiation, reduce permanent deformation, and increase tensile strength (Slebi-Acevedoet al., 2019; Slebi-Acevedo et al., 2020). Several review studies have reported that in conventional HMA, synthetic fibers can improve fatigue resistance, rutting resistance, and sometimes moisture sensitivity, although results depend heavily on the fiber type and dosage (Musa et al., 2019; Slebi-Acevedoet al., 2019).

More recent studies have focused on modern aramid and hybrid fibers. Laboratory evaluations have shown that aramid and polyolefin fibers can improve both rutting and cracking performance in dense-graded asphalt mixtures, especially under heavy traffic conditions (Drašković et al., 2023; Mateos & Harvey, 2019). Research conducted on a typical California mix with 15 percent RAP and aramid fibers reported higher fatigue life and better rutting resistance with minimal changes in volumetrics, which suggests that fiber reinforcement may be useful in high-strain applications such as overlays on concrete pavements (Mateos & Harvey, 2019). Although fiber-reinforced asphalt has shown encouraging results, most published research examines mixtures with RAP only, and there is limited work investigating the combined use of polymer fibers and RAS. There is a clear need to evaluate the combined effects of reclaimed asphalt shingles and polymer fibers in dense-graded hot mix asphalt using performance testing aligned with the Balanced Mix Design framework. The main knowledge gaps include how polymer fibers influence the cracking and rutting behavior of RAS mixtures compared with traditional HMA, whether fiber-reinforced RAS mixtures can meet typical BMD performance thresholds, and what this performance concern means for agencies that want to increase recycled binder content without compromising durability. Understanding these relationships will help determine whether polymer fiber–reinforced RAS mixtures are a feasible option for California and other regions with similar policies and climate conditions.

2. Literature Review

2.1. Introduction

Reclaimed asphalt shingles (RAS) are becoming a popular recycled material in hot mix asphalt (HMA) because they contain a high amount of asphalt binder, typically between 19% and 36% by weight. Using RAS helps reduce the need for virgin materials and keeps construction waste out of landfills (Federal Highway Administration [FHWA], 2022). However, the binder in RAS is highly oxidized and very stiff, which makes the asphalt mix brittle and more likely to crack under repeated loading or cold weather conditions (Riccardi et al., 2023). To prevent premature pavement failure, most transportation agencies limit RAS content to around 5% of the total mix (FHWA, 2022).

Across the United States, only 13 state departments of transportation currently permit the incorporation of RAS into HMA, and even in those jurisdictions, the maximum dosage is generally limited to 5% by total aggregate mass and restricted to post-manufacturer scrap in order to mitigate legacy asbestos risks (Haas et al., 2019). AASHTO PP 78-17 requires solvent recovery of shingle binder to keep the temperature difference above –5 °C, but this adds cost, time, and hazardous solvents. Yan et al. (2018) instead used an enhanced mortar method, blending ground RAS with virgin binder and back-calculating grade change rate (GCR0), matching solvent recovery grades to within 1 °C without solvents.

Laboratory evaluations paint a nuanced picture of RAS's influence on mechanical performance. At high temperatures, both flow-number tests and asphalt-pavement-analyzer trials have indicated that modest additions of RAS can enhance rutting resistance, yet Haas et al. (2019) observed a 59% reduction in semi-circular bend (SCB) flexibility index, underscoring a trade-off with cracking resistance. Because partial binder availability effectively stiffens the asphalt mastic, balanced mix design protocols should incorporate RAS-specific RBA factors and, where feasible, pair higher shingle dosages with softer virgin binders or compatible rejuvenators to maintain critical temperature differentials (ΔT_c) and flexibility (Mocelin et al., 2023).

To reduce the brittleness caused by RAS, researchers have looked at using polymer fibers. Fibers such as aramid, polypropylene (PP), polyester (PET), and basalt are being tested for their ability to strengthen asphalt mixtures with RAS. These fibers spread throughout the asphalt and help bridge small cracks as they form, which may slow crack growth and improve durability. While there is strong agreement that fibers help with rutting resistance at high temperatures, results for fatigue and low-temperature cracking are more mixed. Some studies have shown big improvements in fracture energy or flexibility index, but others have found little to no change (Wiśniewski et al., 2020).

Recently, warm mix asphalt (WMA) technologies also have been shown to increase allowable RAS contents because the lower production temperatures improve workability and density, helping agencies meet both sustainability and resilience targets without sacrificing performance (Sias, 2024b). The following review examines reclaimed asphalt shingles in asphalt mixtures, with fibers discussed only when they are used to address RAS-specific challenges such as oxidized binder, partial blending, and cracking.

2.2. Use of RAS in Asphalt Mixes

Recycled asphalt shingles (RAS) are increasingly used in hot mix asphalt as a source of high binder content and fine aggregate. They help lower material costs and reduce the demand for virgin binder, but the aged and oxidized binder they contain creates a continual trade-off between rutting resistance and cracking susceptibility. Post-consumer shingles usually contain about 19–36% asphalt binder along with fiberglass or cellulose mats, mineral fillers, and sand-sized granules. Even small percentages of RAS therefore introduce a disproportionate amount of stiff binder and fines into the mix (Cooper et al., 2017).

Because of these properties, most agencies limit RAS to only a few percent of total mix mass. Many states also prefer post-manufacturer scrap rather than post-consumer material due to historic asbestos concerns. However, laboratory programs using screened post-consumer shingles have confirmed that stockpiles can be asbestos-free, suggesting that policy could shift toward focusing more on binder quality and balanced performance (Haas et al., 2019).

Mechanically, RAS stiffens both the blended binder and the mixture. In a New Jersey study by Haas et al. (2019), designed under AASHTO PP 78, the inclusion of RAS raised the high, intermediate, and low continuous performance grades of the blended binder and increased mixture stiffness and flow number. These changes improved rutting resistance but also increased the risk of cracking at intermediate and low temperatures. In the same program, the semicircular bend Flexibility Index dropped by nearly 60% with RAS after short-term aging, while Asphalt Pavement Analyzer and AMPT flow-number tests showed performance that met or exceeded the >30 MESALs threshold. This highlighted the typical rutting–cracking trade-off associated with RAS (Haas et al., 2019). The aggregate fraction of RAS was also very fine, with most passing the #8 sieve and more than a quarter passing the #200 sieve, which means gradation control is another concern during design and production.

Field trials in Washington State produced similar results. Mixtures with RAS exhibited higher stiffness and better rutting resistance while maintaining acceptable moisture performance, but they required careful binder selection and volumetric adjustments to manage low-temperature and fatigue cracking risks (Wu et al., 2016). AASHTO PP 78 provides a framework for moving from percentage caps on RAS to performance-based limits on binder replacement. In New Jersey, Haas et al. (2019) showed that maximum allowable contributions from RAS binder were about 18% of total binder for PG 64-22 and 13% for PG 76-22 to avoid excessive embrittlement. Binder tests such as ΔTc, Glover–Rowe, crossover frequency, and R-value confirmed the growing risk of fatigue and durability problems as the proportion of RAS binder increased (Haas et al., 2019).

Beyond binder tests, Balanced Mix Design (BMD) practice usually requires Hamburg Wheel Tracking for rutting and SCB or overlay tests for cracking to make sure both performance targets are met. Larger studies have shown that as RAP and RAS contents rise, cracking indices consistently decline, and softer PG binders alone do not always recover lost durability (Mivehchi et al., 2023). Work on thin-lift overlays further illustrates these trade-offs and shows how warm-mix asphalt (WMA) can help.

In one study, adding 5% RAS alone or with RAP increased mixture stiffness and improved moisture resistance in Hamburg testing, but reflective-cracking resistance dropped compared with the virgin control (Mogawer et al., 2011). Producing the same mixtures with WMA lowered stiffness and partly offset the reflective-cracking penalty without reducing low-temperature performance. Low-temperature cracking device results also showed that mixes with RAS or RAP performed within 1–2 °C of the control, suggesting that for these designs, low-temperature performance could be maintained while WMA or softer binders managed reflective cracking.

Because not all of the binder in RAS becomes available during mixing, and the binder that does blend is very stiff, many agencies have tested recycling agents (RAs) to improve blending and reduce cracking. Screening studies showed that increasing RA dosage softens the binder and shifts chemistry in a favorable direction, but it can also reduce rutting resistance and, at higher levels, harm fracture performance, suggesting dosage must always be set by mixture testing rather than binder testing alone (Aguirre et al., 2017). Focused studies on re-refined engine-oil bottoms (REOB) in 5% RAS mixtures found that REOB raised the recycled binder ratio to nearly 20% of total binder. Hamburg rutting performance remained similar to the control, but fracture energy fell and low-temperature cracking worsened at higher REOB doses, reinforcing the need to cap recycled binder ratio (RBR) and to calibrate RA levels by mixture cracking performance (Cooper et al., 2017).

Other work has shown that MSCR Jnr values are better predictors of rutting performance in high-recycled mixtures than the older G*/sin δ parameter. For instance, a blend of 30% RAP and 5% RAS with 10% REOB met high-temperature grade requirements but showed fewer wheel-tracking passes to 12.5 mm, with Jnr-based targets providing clearer thresholds (Zhang et al., 2021). At the structural level, machine learning models that explicitly include RAS content and mixture volumetrics have been able to predict dynamic modulus (E*) more accurately, improving design reliability compared with empirical models (Liu et al., 2018). Mechanistic-empirical pavement design studies have also confirmed that even PP 78–compliant designs need project-specific verification, since softer binders and rejuvenators do not always restore cracking resistance once RAS is added (Shirzad et al., 2018).

Together, these findings show that RAS can be used reliably at modest levels, provided that binder quality, recycled binder ratio, and cracking tolerance are directly controlled in the design process and verified with performance.

2.3 Use of Polymer Fibers in Asphalt Mixes

Polymer fibers are increasingly used to counter the brittleness introduced by the oxidized, stiff binder in reclaimed asphalt shingles (RAS). High-temperature-stable synthetics such as aramid (e.g., Kevlar) and polyacrylonitrile (PAN) are attractive for structural reinforcement (ASTM, 2023; Riccardi et al., 2023), but achieving uniform dispersion is nontrivial because electrostatic clumping can occur; low-melting polyethylene carrier fibers are often co-fed to separate strands during mixing (Surface Tech, 2025). Cost-effective options such as polypropylene (PP) and polyester (PET) remain common: PP's melting point is close to mixing temperatures, so it can transition from a discrete fiber to a binder modifier, yet improvements in cracking resistance and stability have been reported in dry-mix applications (Tapkin, 2008; Shanbara et al., 2020).

Basalt can raise rutting and cracking resistance via thermal toughness, while glass bonds well but may be too brittle for long-term traffic loads (Zhao et al., 2020); organic cellulose primarily controls drain-down rather than adding structural reinforcement (Riccardi et al., 2023). Recent laboratory work showed synergy from very low–dosage polyolefin/aramid blends (≈0.05%) with sizable gains in dynamic modulus and durability (Khan et al., 2024). Because aged RAS binder complicates fiber–binder adhesion, surface treatments (e.g., Sasobit wax, bitumen emulsions) and systems approaches (e.g., pairing fibers with softer virgin binders or rejuvenators) are used to improve compatibility and balance stiffness versus flexibility (Surface Tech, 2025; Almutairi et al., 2024; Ghabchi et al., 2021). Complementary AMPT-based predictions suggest para-aramid ~0.5 kg t^{-1} can increase asphalt-layer coefficients in fatigue-controlled sections, though rut benefits are less conclusive (Karanam et al., 2024).

Multiple studies indicated rutting improvements when fibers are well selected and dispersed. PP at ~0.3% by aggregate weight raised stiffness ≈30% and improved load-carrying capacity (Shanbara et al., 2020); basalt at ~0.3% increased Marshall stability ~20% and rut resistance >25% (Zhao et al., 2020). Hamburg Wheel Tracking studies have shown that fiber-reinforced RAP mixtures exhibit improved rutting performance (Rahim et al., 2025), recycled PET mixtures maintain rutting resistance (Rangelov et al., 2021), and aramid–polyolefin or aramid–wax fiber blends improve rutting performance compared with control mixtures (Karki et al., 2021). Bamboo-fiber SMA reported 10.4% higher high-temperature stability and 16.9% greater maximum tensile strain than lignin-fiber mixes (Cao et al., 2025). While many datasets emphasize

RAP rather than RAS, the results suggest that fibers can offset high-temperature deformation guides RAS mixture design.

RAS heightens cracking risk due to binder stiffness and partial binder availability, so fatigue/low-temperature performance is pivotal. In high-RAP contexts (informative for RAS design), basalt and polyester fibers improved fatigue life by 135% and increased fracture energy ~14% (Zhu et al., 2024); recycled PET boosted CTindex by ~48% (Rangelov et al., 2021); and intermediate-temperature cracking resistance improved broadly with fiber use (Rahim et al., 2025). Layer-wise optimization (e.g., ~0.3% basalt in surface, ~0.1% in intermediate) can enhance fatigue resistance without penalizing rutting (Xie et al., 2024). However, not all results are positive: Some aramid trials showed modest gains, likely limited by mixing quality and dosage (Wiśniewski et al., 2020). Overall, benefits are conditional on fiber type, dosage, layer placement, and dispersion—factors that interact with RAS binder characteristics.

Agencies increasingly rely on Balanced Mix Design (BMD) to qualify fiber-reinforced, high-recycled mixtures, with Hamburg, IDEAL-CT, and tailored aging protocols used to target rutting and cracking simultaneously (FHWA, 2022b; NAPA, 2025). In practice, BMD allows asphalt mixtures to be adjusted using mechanical-test results, with common strategies including changes to recycled material content, binder grade, binder content, air voids, VMA, aggregate structure, and additives, depending on the specific mixture and agency requirements (Bennert, 2023). Field evidence aligns with lab expectations: At NCAT, a warm-mix, high-RAP section with ~0.15% aramid–polyolefin showed a 58% rut-depth reduction and ~70% fewer surface cracks after >11 million ESALs relative to controls (Leiva-Villacorta & Julian, 2020), and cold-climate pavements with aramid fibers retained PCI 12–15 points higher across two harsh winters (Blankenship & Simons, 2024).

Life-cycle cost analyses (LCCA) indicate that a ~$10–$12 per-ton additive premium can still reduce net present costs ~10–12% over 35 years by extending overlay cycles (FHWA, 2024), while supplier modeling suggests thickness reductions (~10 mm) or overlay deferrals can yield sizable operational and carbon savings (Surface Tech, 2024). Reliable outcomes hinge on accurate dosing and dispersion (pelletized/pre-blended products) and verification via ignition-oven residue testing per ASTM D8395-23 (ASTM, 2023). Specification gaps can be narrowed by explicitly referencing AASHTO PP 105-20 and FHWA performance thresholds (FHWA, 2022b), supported by workforce training and mechanistic-economic evidence showing multi-fold overlay cost-effectiveness for aramid-fiber mixes (Harder, 2023; Bastola et al., 2020).

RAS displaces virgin binder/aggregate and diverts significant waste from landfills, improving resource efficiency and embodied impacts. EPD data indicate ~65 g/t para-aramid contributes ~2.4 kg CO_2-e per ton of mix, which is typically offset by 18–25 kg CO_2-e saved via RAS binder replacement, yielding a ~6–12% net emissions reduction (SCS Global Services, 2023). Pairing

WMA with high RAS can further reduce the carbon footprint and aligns with industry roadmaps toward net-zero emissions by 2050 (NAPA, 2024 March). For post-consumer RAS, asbestos compliance per federal and state rules remains essential (FHWA, 2022).

Production-scale programs demonstrate that fiber-reinforced high-recycled mixes can exceed BMD thresholds and enable pay-for-performance strategies. Pennsylvania's NECEPT work reported Hamburg and IDEAL-CT margins of 20–40% above thresholds with 0.5-inch thickness reduction potential (NECEPT, 2024). NCAT Phase VIII (2021–2024) documented 63% less rut depth and a 2-year delay in first cracking for 0.15% aramid-polyolefin sections versus high-RAP controls (NCAT, 2024). Additional deployments showed 45% fewer reflective cracks in New York composite pavements treated with poly-aramid (Noorvand, 2024); thin basalt-fiber overlays maintained dynamic modulus ~25% higher after 18 months (Li et al., 2023); and ceramic-fiber WMA halved permanent deformation in 30% RAP mixes (Obaid et al., 2024). Airports and heavy-duty yards reported simultaneous stiffness and fatigue gains with polyolefin/aramid hybrids and successful use of steel fibers at high RAP without debonding (Khan et al., 2024; Nian et al., 2024).

Multi-year PCI advantages on Kentucky's Dixie Highway corroborate durability benefits (Blankenship et al., 2024). Cold-region innovations include chemically modified cotton-straw fibers in micro-surfacing (60% winter ravelling reduction) and 100% RAP cold mixes with ~0.30% PP meeting Marshall stability for secondary highways (Zhao et al., 2024; Valderrama Solano et al., 2024). Mechanistic work with DOT-approved aramid dense-graded mixes strengthens lab-to-field stiffness correlations and supports thickness design adjustments within BMD frameworks (Karanam & Underwood, 2024). Although many of these demonstrations are RAP-focused, their implementation templates (dosage windows, QA/QC, performance criteria, thickness crediting) translate directly to RAS mixtures when RAS-specific binder availability and asbestos protocols are addressed.

Despite broad RAP/fiber literature, direct RAS + fiber datasets remain limited; targeted RAS trials are needed to quantify fatigue and thermal-cracking benefits and to calibrate BMD criteria. Plant-scale dispersion metrics are not standardized, and aging/moisture responses vary by fiber chemistry (Zhang et al., 2023; Lin et al., 2023). In multi-recycled systems, binder-replacement credits can be offset by high-temperature fiber production impacts, underscoring the need for harmonized LCA functional units (Abdalla et al., 2022). Divergent low-temperature fracture responses (basalt vs. glass) are not fully captured in current BMD protocols (Serin et al., 2023). Finally, aramid form factor (pulp, powder, staple) alters rheology differently, with sparse field correlations to guide specification writing (Zhao et al., 2025).

2.4 Conclusion

Reclaimed asphalt shingles (RAS) provide sustainability and cost benefits but are limited by the brittleness of their aged binder. While RAS improves rutting resistance, it reduces flexibility and increases cracking risks, requiring balanced mix design approaches. Polymer fibers such as aramid, polypropylene, polyester, and basalt show strong potential to offset these drawbacks, especially when paired with warm-mix asphalt, softer binders, or rejuvenators. Although most findings come from RAP contexts, early field trials confirm that fiber-reinforced high-recycled mixtures can meet performance thresholds and extend service life. Expanding targeted RAS and fiber research together and refining specifications will be key to enabling broader, performance-based use of RAS in durable, sustainable pavements.

3. Objectives

The objective of this project is to evaluate the mechanical performance of hot mix asphalt mixtures modified with reclaimed asphalt shingles and two commercial polymer fibers. This study examines how fiber type and dosage influence the performance of RAS modified mixtures and whether fiber reinforcement can help balance rutting and cracking behavior.

The research included two RAS contents (3% and 5% by total mix weight) and two commercial polymer fibers (designated as Fiber A and Fiber B). Each fiber type was added at three dosages (0.05%, 0.10%, and 0.15% of total mix weight). For each RAS level, a mixture without fibers served as the control. This resulted in seven mixtures per RAS group and 14 mixtures in total. All mixtures were evaluated using the Hamburg Wheel Tracking Test to assess rutting resistance and the IDEAL Cracking Test to assess cracking resistance. To achieve the objective of this study, the following comparisons were made:

1. Rutting resistance of mixtures containing different RAS contents, fiber types, and fiber dosages using the Hamburg Wheel Tracking Test.
2. Cracking resistance of mixtures containing different RAS contents, fiber types, and fiber dosages using the IDEAL Cracking Test.
3. Performance of Fiber A and Fiber B at equivalent dosages to determine whether fiber type influences rutting or cracking behavior.
4. Each fiber-reinforced mixture with its corresponding RAS-only control mix to determine whether polymer fibers improve the brittleness associated with RAS.
5. Overall trends across all mixtures to identify the RAS fiber combinations that provide the most balanced performance between rutting resistance and cracking resistance.

Through these comparisons, the study aimed to determine whether polymer fibers can effectively enhance the performance of RAS modified asphalt mixtures and support the development of more durable and sustainable pavement materials.

4. Experimental Work and Results

This study aimed to evaluate the effectiveness of a commercially available polymer fiber in enhancing the mechanical performance of hot-mix asphalt (HMA) incorporating varying proportions of recycled asphalt shingles (RAS). Rutting and moisture damage resistance were assessed using the Hamburg Wheel Tracking (HWT) test in accordance with AASHTO T 324-23, while intermediate-temperature cracking resistance was evaluated using the Cracking Tolerance Index (CTI) test following ASTM D8225-19. Aggregates and RAS materials used in a Caltrans-approved HMA mixture for a Route 4 project in Concord, California, were provided along with the corresponding job mix formula (JMF). This chapter describes the physical properties of the materials, the JMF, and the results obtained from the HWT and CTI tests.

4.1 Aggregate Properties

4.1.1 Mix With 3% RAS

Virgin and RAS aggregates used in HMA mixes commonly used in projects in the Bay Area of California were used with mixes containing 3% RAS and were supplied by Granite Construction from their HMA production plant located in Paso Robles, California. The aggregate properties are presented in Table 1.

Table 1. Properties of Aggregate Used for the 3% RAS Mix

Property	Test Method	Test Results	Specification[1]
Crushed coarse aggregate, One fractured face, %	AASHTO T 335	98	95
Crushed coarse aggregate, Two fractured faces, %	AASHTO T 335	99	90
Crushed fine aggregate, One fractured face, %	AASHTO T 335	96	40
Los Angeles abrasion, loss at 100 revolutions, %	AASHTO T 96	5	12
Los Angeles abrasion, loss at 500 revolutions, %	AASHTO T 96	17	40
Sand equivalent	AASHTO T 176	80	47
Flat and elongated particles (% by mass at 5:1)	ASTM D 4791	0	10
Bulk specific gravity of coarse aggregate	AASHTO T 85	2.64	NA[2]
Absorption of coarse aggregate	AASHTO T 85	1.3	NA
Bulk specific gravity (SSD) of fine aggregate	AASHTO T 84	2.66	NA
Bulk specific gravity of fine aggregate	AASHTO T 84	2.54	NA
Apparent specific gravity of fine aggregate	AASHTO T 84	2.76	NA
Apparent specific gravity of supplemental fines	AASHTO T 84	-	NA
Absorption of fine aggregate	AASHTO T 84	1.3	NA
Bulk specific gravity of aggregate blend	SP-2 Asphalt Mix	2.666	NA

[1] Following Caltrans 2024 Standard Specifications
[2] NA = Not Available

Table 2 and Figure 1 present the aggregate and blend gradations.

Table 2. Aggregate and Blend Gradation

Sieve Size	Bin #1 (3/4" CR)	Bin #2 (1/2" CR)	Bin #3 (3/8" CR)	Bin #4 (1/4" Chips)	Bin #5 (Mfd. Sand)	RAP (25%)	RAS (3%)	Combined Blend
2"	100	100	100	100	100	100	100	100
1 1/2"	100	100	100	100	100	100	100	100
1"	100	100	100	100	100	100	100	100
3/4"	95	100	100	100	100	100	100	99
1/2"	14	79	100	100	100	100	100	82
3/8"	4	23	90	100	100	100	100	73
No. 4	3	4	16	85	96	85	–	52
No. 8	2	3	6	4	70	64	–	34
No. 16	2	2	3	1	43	47	–	23
No. 30	2	2	3	1	28	36	–	17
No. 50	1	2	2	1	16	26	–	11
No. 100	1	1	2	0	8	19	–	7
No. 200	0.6	0.7	0.9	0.3	4.1	14.1	–	5

Figure 1. FHWA 0.45 Power Gradation Chart for 3% RAS Blend

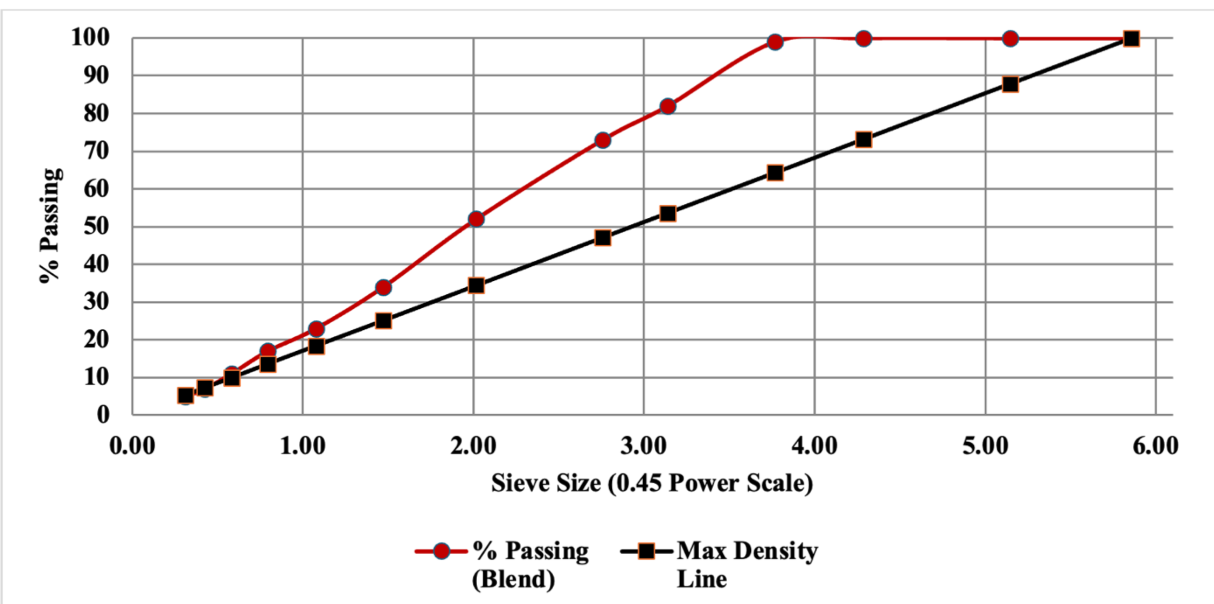

Mix With 5% RAS

Virgin and RAP aggregates used in HMA mixes commonly used in projects in the Bay Area were used with mixes containing 25% RAP and were supplied by Granite Construction from their HMA production plant located in Salinas, California. Their different properties are presented in Table 3.

Table 3. Properties of Aggregate Used for the 5% RAS Mix

Property	Test Method	Test Results	Specification1
Crushed coarse aggregate, One fractured face, %	AASHTO T 335	99	95
Crushed coarse aggregate, Two fractured faces, %	AASHTO T 335	97	90
Crushed fine aggregate, One fractured face, %	AASHTO T 335	99	40
Los Angeles abrasion, loss at 100 revolutions, %	AASHTO T 96	5	12
Los Angeles abrasion, loss at 500 revolutions, %	AASHTO T 96	20	40
Sand equivalent	AASHTO T 176	76	47
Flat and elongated particles (% by mass at 5:1)	ASTM D 4791	0	10
Bulk specific gravity of coarse aggregate	AASHTO T 85	2.64	NA2
Absorption of coarse aggregate	AASHTO T 85	1.55	NA
Bulk specific gravity (SSD) of fine aggregate	AASHTO T 84	2.7	NA
Bulk specific gravity of fine aggregate	AASHTO T 84	2.66	NA
Apparent specific gravity of fine aggregate	AASHTO T 84	2.78	NA
Absorption of fine aggregate	AASHTO T 84	1.61	NA
Bulk specific gravity of aggregate blend	SP-2 Asphalt Mix	2.66	NA

1 Following Caltrans 2024 Standard Specifications
2 NA = Not Available

Table 4 and Figure 2 present the gradation of individual aggregate fractions and the aggregate blend.

Table 4. Gradation of Individual Aggregate Fractions and Blend

Sieve Size	Bin #1	Bin #2	Bin #3	Bin #4	Bin #5 (Mfd. Sand)	RAP (25%/5% RAS)	–
2"	100	100	100	100	100	100	100
1 1/2"	100	100	100	100	100	100	100
1"	100	100	100	100	100	100	100
3/4"	95	100	100	100	100	100	98
1/2"	14	79	100	100	100	100	83
3/8"	4	23	90	100	100	99.8	74
No. 4	3	4	16	85	96	85	52
No. 8	2	3	6	4	70	64	33
No. 16	2	2	3	1	43	47	22
No. 30	2	2	3	1	28	36	15
No. 50	1	2	2	1	16	26	10
No. 100	1	1	2	0	8	19	6
No. 200	0.6	0.7	0.9	0.3	4.1	14.1	4.3

Figure 2. FHWA 0.45 Power Gradation Chart for 25% RAP Blend

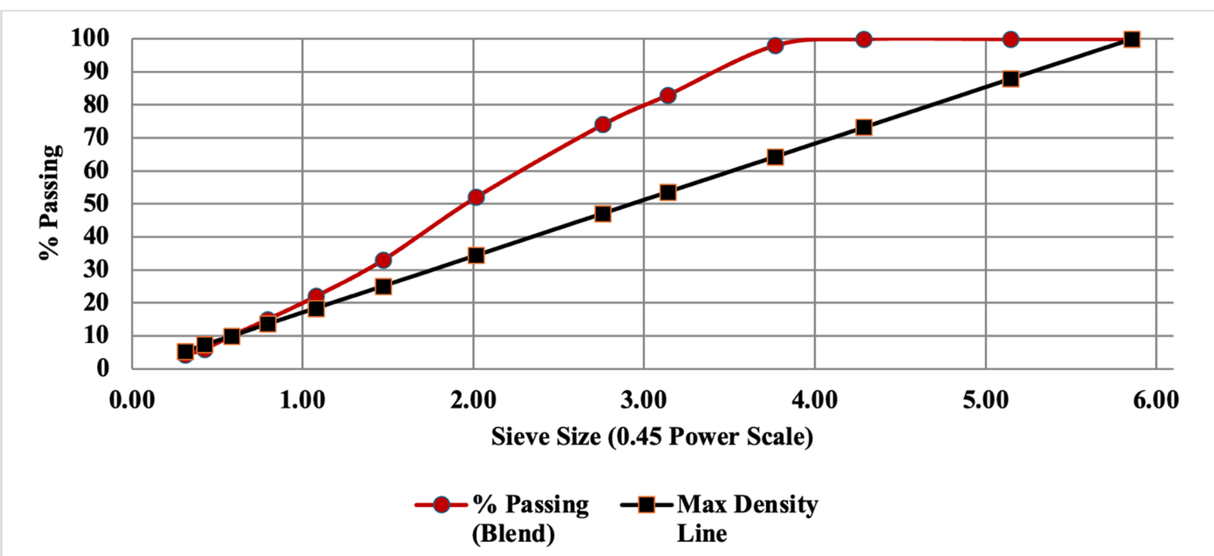

4.2 Asphalt Binder Tests and Results

A performance grade PG 58-22 asphalt binder was used in this study. The binder was supplied by Valero and incorporated into a 3/4 in. HMA Type A mix produced by Granite Construction. This binder selection is consistent with Caltrans's practice for surface course mixtures in California and aligns with the approved contractor mix design.

The binder properties were obtained from the Caltrans Contractor Hot Mix Asphalt Design Data form (DOT CEM-3512). The specific gravity of the PG 58-22 binder was measured in accordance with AASHTO T 228 and was reported as 1.0264. The high temperature rheological performance of the binder was evaluated using a Dynamic Shear Rheometer following AASHTO T 315 on Rolling Thin Film Oven aged residue. The measured G*/sinδ value was 3.92 kPa at the specified test temperature, which exceeds the Caltrans minimum requirement of 2.20 kPa for PG 58-22 binders.

The supplier recommended a mixing temperature range of 289 °F to 299 °F. An amine-based recycling agent and antistrip additive, Evoflex X1, was included at a dosage of 2.0% by weight of asphalt binder. The antistrip source was Ingevity, and the binder met all applicable Caltrans Section 92 requirements for treated asphalt binders.

Table 5. Binder Properties

Property	**Test Method**	**PG 58-22**
Specific Gravity	AASHTO T 228	1.0264
Dynamic Shear (RTFO Residue)	AASHTO T 315	3.92 kPa (G*/sinδ at 58 °C, RTFO residue)

4.3 Polymer Fiber

Two polymer fibers recently implemented in a Caltrans maintenance project on State Route 1 were evaluated in this study. The fibers are designated as Fiber A, which is wax coated, and Fiber B, which is non coated and treated with a liquid emulsion. The material properties of both fiber types are summarized in Table 6, and representative images of the fibers are presented in Figure 3.

Figure 3. Aramid Fiber Type A and Type B

Table 6. Properties of Fiber Type A and Type B

Property	Fiber Type A	Fiber Type B
Material	Para-Aramid (min 63% by weight)	Para-Aramid (min 75% by weight)
Treatment	Wax (max 37% by weight)	Liquid emulsion binder (max 25% by weight)
Standard Dose	**2.1 oz per US ton of asphalt mix**	**2.1 oz per US ton of asphalt mix**
Decomposition Temp	>800 °F / 425 °C	>800 °F / 425 °C
Linear Density	>3200 dtex (ASTM D1907/1907M-12)	>3200 dtex (ASTM D1907-12, OPT6)
Length	**¾ in (19 mm) or 1.5 in (38 mm), ±10%**	**¾ in (19 mm) or 1.5 in (38 mm), ±10%**
Color	Yellow	Yellow
Tensile Strength	>2700 MPa (ASTM D2256, D7269)	>2700 MPa (ASTM D2256, D7269)
Young's Modulus	**>80 GPa (ASTM D2256, D7269)**	**>80 GPa (ASTM D2256, D7269)**

Note. Bolded properties were identical across fiber types.

4.4 Uncompacted Asphalt Mix Tests

All mixtures used in this study were produced using a constant reclaimed asphalt pavement content of 25% by total aggregate weight. The experimental variables consisted of reclaimed asphalt shingles incorporated at 2 levels (3% and 5% by total mix weight) along with the inclusion of polymer fibers. The control HMA and fiber modified HMA differed only in fiber and RAS contents, while all other mixture properties and volumetric parameters were maintained constant.

The Job Mix Formula for the base HMA containing 25% RAP was provided by the material supplier. A single optimum binder content of 5.2% by total mix weight was used for all mixtures evaluated in this study. Three fiber dosages of 0.05%, 0.10%, and 0.15% by total mix weight of both Fiber A and Fiber B, respectively, were investigated. All mixtures incorporated a liquid antistripping additive at a dosage rate of 0.5% by weight of the asphalt binder.

4.5 Theoretical Maximum Specific Gravity (AASHTO T 209)

The theoretical maximum specific gravity was determined for each mixture and is a key parameter used to calculate air void content in compacted specimens prepared for subsequent performance testing as shown in Figure 4. Loose asphalt mixtures representing each combination of RAS content and fiber dosage were prepared and conditioned for 2 hours. Following conditioning, the mixtures were allowed to cool in an uncompacted state and then placed in a vacuum container filled with water.

A high vacuum pump was connected to the container and operated for a minimum duration of 20 minutes to remove entrapped air. During vacuum saturation, the container was intermittently agitated to assist in releasing air bubbles from the mixture. After vacuum saturation, the container was removed from the pump and filled with water to the calibrated level. The mass of the container with the specimen and water was recorded. This value, along with the dry mass of the specimen and the mass of the container filled with water only, was used to calculate the theoretical maximum specific gravity (TMSG) in accordance with AASHTO T 209. TMSG was determined using the following relationship:

$$TMSG = A / (A + B - C)$$

where A = mass of oven-dried specimen (g), B = mass of container filled with water at 25^{o} C (g), and C = mass of container filled with specimen and water (g). The theoretical maximum specific gravity for both mixtures was found to be 2.509, indicating no significant change in theoretical density with the increase in RAS content.

Figure 4. TMSG Test Setup

4.6 Preparation of Specimens for Hamburg Wheel Tracking (HWT) and Cracking Tolerance Index (CTI) Tests

Specimens for the Hamburg Wheel Tracking and Cracking Tolerance Index tests were prepared using a Superpave Gyratory Compactor in accordance with AASHTO T 312. All specimens had a nominal diameter of 150 mm. Target specimen heights were 60 ± 1 mm for Hamburg testing and 62 ± 1 mm for CTI testing.

The specimen preparation procedure included drying aggregates to constant mass; batching aggregate components; heating aggregates and binder to the designated mixing temperature; blending aggregates with binder, fibers, and RAS; short term conditioning; and compacting specimens to the target air void level using the gyratory compactor.

Aggregates and RAP were weighed separately in steel pans and combined to achieve the desired batch mass. For Hamburg testing, aggregate batches of approximately 5,250 g were prepared to fabricate two specimens per batch. The required quantity of RAS was then added based on the target RAS percentage of 3% or 5% by total mix weight.

The combined aggregates, RAP, and RAS were heated in an oven to the appropriate mixing temperature based on the performance grade of the asphalt binder. The asphalt binder was heated separately to the same temperature. Once the materials reached the target temperature, the aggregates were placed into a mechanical mixer, and a crater was formed. The liquid antistripping additive was first blended with the asphalt binder, followed by the addition of the binder to the aggregate blend. Fiber additives were then introduced, and mixing continued until all aggregate particles and fibers were uniformly coated with binder.

The mass of loose mixture required to produce compacted specimens with a target air void content of 7 ± 0.5% was determined theoretically using the relationship:

$$W = \%G_{mm} \text{ at } N_f \times G_{mm} \times \text{specimen volume}$$

where %Gmm at Nf equals 0.93 for Hamburg specimens, Gmm is the theoretical maximum specific gravity of the loose mixture, and specimen volume was calculated using a specimen diameter of 150 mm and heights of 60.2 mm for Hamburg specimens and 62 mm for CTI specimens.

To refine the target specimen mass, three trial specimens were compacted using mixture masses of W, W + 10 g, and W − 10 g. The Superpave Gyratory Compactor was used to compact the specimens to the target height, and the resulting air void contents were calculated. The mixture mass that produced specimens within the required air void range was selected for final specimen fabrication. Specimens prepared for Hamburg testing were saw cut, and the amount of material removed was adjusted to achieve a gap of 4 mm ± 3 mm between molds at the start of testing.

Fiber dispersion was visually checked in loose mix samples before compaction to ensure specimen integrity. Clumping can increase variability and affect performance results (Noorvand et al., 2022). Studies have shown better dispersion improves cracking resistance consistency (Karanam & Underwood, 2024). Batches with poor dispersion were discarded and remade to maintain consistency across all mixes. Figures 5–8 show the mixture preparation and specimen fabrication sequence: a representative batch of loose mixture (Figure 5), the mechanical mixer used to produce it (Figure 6), the Superpave Gyratory Compactor used to compact the specimens (Figure 7), and the resulting compacted specimens prepared for Hamburg Wheel Tracking testing (Figure 8).

Figure 5. Mixture Batches

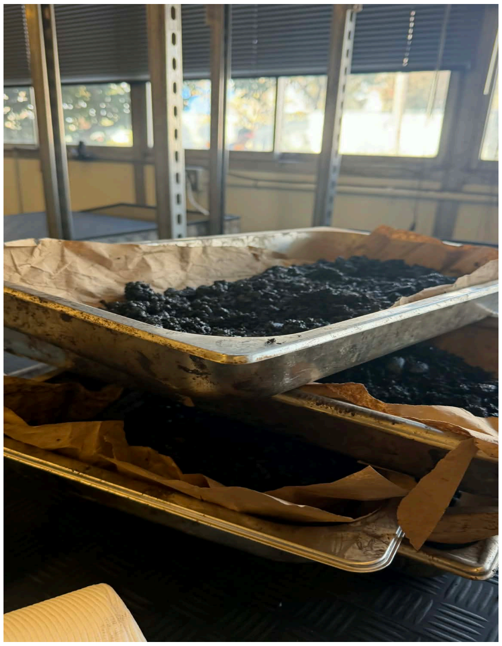

Figure 6. Mechanical Mixer

Figure 7. SG Compactor

Figure 8. Specimens for HWT

4.7 Bulk Specific Gravity and Air Void Determination

Bulk specific gravity and air void content were determined for all compacted asphalt mixture specimens to verify compliance with target volumetric requirements and to support subsequent performance testing. These measurements were required to confirm specimen quality prior to Hamburg Wheel Tracking and Cracking Tolerance Index testing.

Bulk specific gravity of compacted specimens was determined in accordance with AASHTO T 166 using the saturated surface dry method. After gyratory compaction, specimens were allowed to cool to room temperature. Each specimen was dried to constant mass when required and weighed in air to obtain the dry mass. The specimen was then submerged in a water bath maintained at approximately 25 °C and weighed while suspended in water to obtain the immersed mass, designated as C. Following immersion, the specimen was surface dried using a damp cloth and immediately weighed in air to determine the saturated surface dry mass.

The bulk specific gravity, Gmb, was calculated using the following relation:

$$Gmb = D / (E - F)$$

where D is the mass of the dry specimen in air (g), E is the mass of the saturated surface dry specimen in air (g), and F is the mass of the specimen in water (g).

Theoretical maximum specific gravity, Gmm, previously determined for each mixture in accordance with AASHTO T 209, was used to calculate the air void content of the compacted specimens. Air voids were calculated in accordance with AASHTO T 269 using the following relationship:

$$Va = 100 \times (1 - Gmb / Gmm)$$

where Va is the air void content of the compacted mixture (%), Gmb is the bulk specific gravity of the compacted specimen, and Gmm is the theoretical maximum specific gravity of the loose mixture. The target air void content for all specimens was 7.0 ± 0.5%. Trial compactions were conducted as necessary to adjust the mass of loose mixture until specimens met the specified air void range. Specimens that did not satisfy the air void requirement were excluded from further testing. Only specimens meeting the target air void criteria were accepted for Hamburg Wheel Tracking and Cracking Tolerance Index testing.

4.8 Hamburg Wheel Tracker (HWT) Test (AASHTO T324)

The Hamburg Wheel Tracking test conducted in this study followed the procedures outlined in AASHTO T 324. The testing device was manufactured by James Cox and Sons, Inc. and was housed at the laboratory facility used for this project. Compact specimens were first cut using a masonry saw and cutting template to ensure proper dimensions for placement within the Hamburg polyethylene molds.

Following cutting, specimens were placed into the polyethylene molds, secured within the mounting tray, and submerged in the Hamburg wheel tracker water bath. The water bath temperature was set to 113 ± 2 °F, equivalent to 45 ± 1 °C, corresponding to the use of a PG 58-22 asphalt binder. Once the target temperature was reached, specimens were conditioned in the water bath for an additional 30 minutes prior to testing.

After conditioning, the steel wheel assemblies were lowered onto the specimen surfaces and the test was initiated. The device applied repeated wheel passes under a constant load while specimens remained submerged. The test was automatically terminated when either the preset maximum rut depth or the maximum number of wheel passes was reached.

Vertical deformation was continuously measured using linear variable differential transducers mounted on both sides of the apparatus. Rut depth data were recorded using an automated data acquisition system. Performance indicators, including post compaction consolidation, creep slope, stripping inflection point, and stripping slope, were derived from the relationship between rut depth and number of wheel passes.

Post compaction consolidation was defined as the deformation measured at 1,000-wheel passes and represents initial densification of the mixture. The creep slope was calculated as the inverse of the deformation rate in the linear region prior to the onset of stripping and reflects rutting behavior dominated by plastic flow. The stripping inflection point corresponds to the wheel pass number at which moisture-related damage initiates, while the stripping slope represents the inverse of the deformation rate after this point and is associated with moisture induced rutting behavior.

Results for the rut depth for all sample combinations are shown in Tables 7 and 8. Results for the stripping property in terms of the number of wheel paths at stripping inflection point are shown in Tables 9 and Table 10. Figures 9–12 show the specimen preparation and testing sequence for the Hamburg Wheel Tracking test: saw-cutting the specimen along its edge (Figure 9), the resulting perpendicular cut face used to seat the specimen in the mold (Figure 10), the Hamburg Wheel Tracker used for testing (Figure 11), and representative specimens after completion of the test (Figure 12).

Figure 9. Saw-Cutting Specimen Along its Edge

Figure 10. HWT Specimen With Perpendicular Cut

Figure 11. Hamburg Wheel Tracker (HWT)

Figure 12. Specimens After HWT Test

Table 7. Rut Depth for HMA with 3% RAS (15,000 Wheel Passes)

Fiber Type	Fiber %	Left side (mm)	Right side (mm)	Average per set (mm)	Total average (mm)
Control	0	4.48	3.67	4.08	3.66
Control	0	2.71	3.79	3.25	
Type A	0.05	4.56	3.66	4.11	3.24
Type A	0.05	2.13	2.59	2.36	
Type A	0.1	2.26	2.84	2.55	2.80
Type A	0.1	3.53	2.55	3.04	
Type A	0.15	3.55	2.71	3.13	2.94
Type A	0.15	2.5	2.98	2.74	
Type B	0.05	2.96	3.09	3.03	3.11
Type B	0.05	3.26	3.12	3.19	
Type B	0.1	2.78	3.17	2.98	2.89
Type B	0.1	2.93	2.69	2.81	
Type B	0.15	2.2	3.37	2.79	2.79
Type B	0.15	2.5	3.1	2.80	

Table 8. Rut Depth for HMA with 5% RAS (15,000 Wheel Passes)

Fiber Type	Fiber %	Left side (mm)	Right side (mm)	Average per set (mm)	Total average (mm)
Control	0	2.45	3.38	2.92	2.87
Control	0	2.79	2.84	2.82	
Type A	0.05	2.38	2.77	2.58	2.56
Type A	0.05	2.74	2.34	2.54	
Type A	0.1	2.56	2.48	2.52	2.41
Type A	0.1	2.18	2.42	2.30	
Type A	0.15	2.66	2.06	2.36	2.41
Type A	0.15	2.61	2.3	2.46	
Type B	0.05	1.93	1.76	1.85	1.87
Type B	0.05	1.94	1.86	1.90	
Type B	0.1	1.96	3.93	2.95	2.73
Type B	0.1	1.53	3.5	2.52	
Type B	0.15	1.81	2.53	2.17	2.15
Type B	0.15	2.42	1.85	2.14	

Table 9. Number of Wheel Paths at Inflection Point for HMA with 3% RAS

Fiber Type	Fiber %	Left side (passes)	Right side (passes)	Average per set (passes)	Total average (passes)
Control	0	NA[1]	NA	NA	NA
Control	0	NA	NA	NA	
Type A	0.05	14,508	NA	NA	NA
Type A	0.05	10,913	13,878	12,396.00	
Type A	0.1	NA	NA	NA	NA
Type A	0.1	NA	17,906	NA	
Type A	0.15	NA	NA	NA	NA
Type A	0.15	16,130	16,149	16,140.00	
Type B	0.05	NA	NA	NA	NA
Type B	0.05	NA	13,538	NA	
Type B	0.1	NA	NA	NA	NA
Type B	0.1	19,866	17,080	18,473.00	
Type B	0.15	NA	18,985	NA	NA
Type B	0.15	16,457	13,987	15,222.00	

[1] NA = Data Not Available.

Table 10. Number of Wheel Paths at Inflection Point for HMA with 5% RAS

Fiber Type	Fiber %	Left side (passes)	Right side (passes)	Average per set (passes)	Total average (passes)
Control	0	18,643.00	NA	NA	NA
Control	0	NA	14,744.00	NA	
Type A	0.05	NA	30,134.00	NA	NA
Type A	0.05	18,898.00	18,881.00	18,890.00	
Type A	0.1	18,735.00	25,889.00	22,312.00	NA
Type A	0.1	NA	18,989.00	NA	
Type A	0.15	20,499.00	NA	NA	NA
Type A	0.15	17,956.00	NA	NA	
Type B	0.05	20,902.00	14,911.00	17,907.00	NA
Type B	0.05	17,645.00	NA	NA	
Type B	0.1	18,362.00	19,826.00	19,094.00	NA
Type B	0.1	11,749.00	NA	NA	
Type B	0.15	NA	NA	NA	NA
Type B	0.15	NA	NA	NA	

[1] NA = Data Not Available.

4.9 Cracking Tolerance Index (CTI) Test (ASTM D8225)

The cracking resistance of each asphalt mixture was evaluated in accordance with ASTM D8225 using the IDEAL Cracking Test. Testing was conducted with Pavetest's Dynamic Loading System, shown in Figure 13, which is a precision-controlled device designed for evaluating asphalt mixture performance under simulated traffic loading. The system includes a vertical axial loading assembly with steel loading plates, a calibrated load cell, displacement measurement instruments, and guide rods to maintain proper alignment. All components are housed within a temperature controlled environmental chamber, and data acquisition and control are managed through integrated software that continuously records test parameters.

Each specimen was compacted using a Superpave Gyratory Compactor to produce cylindrical samples with a diameter of 150 mm and a thickness of 62 mm. The air void content of all specimens was carefully controlled to achieve a target value of 7.0% with an allowable tolerance of ± 0.5%. FPrior to testing, the specimens were conditioned inside an environmental chamber at the designated intermediate temperature. Conditioning temperatures were set to 22 °C for all mixtures evaluated in this study, which contained 25% RAP. All specimens were conditioned for 120 ± 10 minutes following the procedures outlined in ASTM D8225-19.

The intermediate test temperature was determined using Equation 1, which relates the intermediate performance grade temperature to the high and low climatic performance grade temperatures of the binder:

$$PG, IT = \frac{PG, HT + PG, LT}{2} + 4 \qquad (1)$$

where PG, IT = intermediate performance grade temperature (°C), PG, HT = climatic high-performance grade temperature (°C), and PG, LT = climatic low-performance grade temperature (°C).

After conditioning, specimens were immediately transferred from the chamber and positioned at the center of the indirect tensile cracking test fixture, as illustrated in Figure 13. A reference line was drawn along the specimen diameter at mid height to ensure accurate alignment within the testing frame. Prior to each test, the loading plates and fixtures were thoroughly cleaned to remove any dust, debris, or residual binder that could affect load transfer or measurement accuracy. Once placed in the fixture, specimens were aligned to ensure uniform contact between the loading strips and specimen surface.

Figure 13. IDEAL-CT Specimen Prepared for Testing

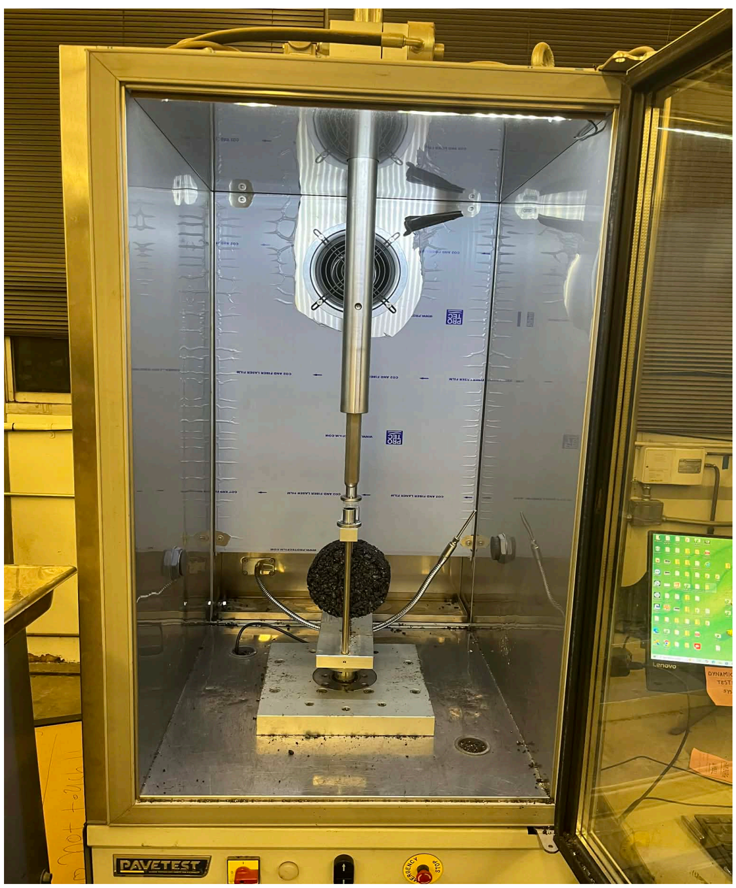

The test fixture consisted of concave steel loading strips with radii matching that of the specimen, allowing for uniform stress distribution along the contact edges. The indirect tensile cracking test was performed by applying axial loading at a constant load line displacement rate of 50 mm per minute. Displacement was measured using sensors with a resolution of at least 0.01 mm. Load and displacement data were recorded continuously at a minimum sampling rate of 40 data points per second to generate smooth and accurate load displacement curves.

Loading continued at the prescribed displacement rate until complete specimen failure occurred. Failure was defined as the point at which the measured load dropped below 100 N. The total testing time for each specimen was maintained within 4 minutes from removal from the conditioning chamber to test completion to minimize any potential effects of temperature fluctuation on test results. The testing software generated graphical load displacement curves and exported numerical data, including load, displacement, and time, into spreadsheet format. These data were then used to calculate parameters related to cracking resistance.

The work of failure, Wf, expressed in Joules, was calculated as the area under the load displacement curve using Equation 2:

$$W_f = \sum_{i=1}^{n-1} [(l_{i+1} - l_i)P_i + ½ (l_{i+1} - l_i)(P_{i+1} - P_i)] \quad (2)$$

where W_f = work of failure (Joules), P_i = applied load (kN) at the i-load step application, P_i+1 = applied load (kN) at the i + 1 load step application, l_i = LLD (mm) at the i step, and l_i+1 = LLD (mm) at the i + 1 step.

The failure energy, Gf, which represents the energy required to initiate and propagate cracking, was calculated by normalizing the work of failure by the specimen cross sectional area using Equation 3:

$$G_f = \frac{W_f}{D * t} \times 10^6 \quad (3)$$

where G_f = failure energy (J/m^2), W_f = work of failure (J), D = specimen diameter (mm), and t = specimen thickness (mm).

The primary performance indicator obtained from the IDEAL Cracking Test is the Cracking Tolerance Index, Ctindex, which characterizes the fatigue cracking resistance of the asphalt mixture. The Ctindex was calculated using parameters derived from the load displacement curve, including the absolute value of the post peak slope between 85% and 65% of the peak load, and the displacement corresponding to 75% of the peak load after the peak. The Ctindex was calculated using Equation 4:

$$CTIndex = \frac{t}{62} \times \frac{l_{75}}{D} \times \frac{G_f}{|m_{75}|} \times 10^6 \quad (4)$$

where CT_{Index} = cracking tolerance index, G_f = failure energy (J/m^2), $|m_{75}|$ = absolute value of the post-peak slope m_{75} (N/m), and l_{75} = displacement at 75 % of the peak load after the peak (mm).

The IDEAL Cracking Test was conducted on all asphalt mixtures with varying reclaimed asphalt pavement contents and fiber dosages. The resulting Ctindex values, along with all associated parameters, are summarized in Tables 11 and 12.

Table 11. IDEAL-CT Test Results for 3% RAS Asphalt Mixtures Modified with Varying Fiber Types and Dosages

Sample name	Sample	Air-Voids	Peak load (kN)	I75(mm)	|m75| (N/m)	W_f (J)	G_f (J/m^2)	CT_{index}	CoV(%)*	*p-value
Control Mix (CM)	1	7.1	17.19	4.84	4.82E+06	91.60	9849.60	65.91	24.18	N/A
	2	6.9	17.16	5.41	6.22E+06	96.18	10341.83	60.02		
	3	7.3	15.77	5.31	7.19E+06	76.22	8195.49	40.32		
	Average		**16.71**	**5.19**	**6.08E+06**	**88.00**	**9462.31**	**55.42**		
A-0.05	1	7	17.56	5.20	6.49E+06	98.92	10636.67	56.85	32.54	0.273
	2	7.3	17.55	4.52	8.32E+06	81.21	8732.52	31.62		
	4	7.4	18.64	4.79	8.44E+06	88.30	9495.06	35.93		
	Average		**17.92**	**4.84**	**7.75E+06**	**89.48**	**9621.42**	**41.47**		
A-0.1	1	6.9	17.39	5.48	6.86E+06	83.37	8964.47	47.71	27.89	0.275
	3	7	19.31	5.00	6.97E+06	98.18	10557.16	50.52		
	4	6.6	20.09	4.44	1.01E+07	91.65	9854.58	28.80		
	Average		**18.93**	**4.97**	**7.98E+06**	**91.07**	**9792.07**	**42.34**		
A-0.15	1	7.4	18.32	4.96	6.08E+06	116.26	12501.25	67.96	20.02	0.357
	3	6.6	18.82	4.62	6.28E+06	100.26	10780.97	52.86		
	4	7.5	18.02	4.44	4.15E+06	103.66	11146.62	79.52		
	Average		**18.39**	**4.67**	**5.50E+06**	**106.73**	**11476.28**	**66.78**		
B-0.05	1	7.3	16.14	6.08	4.76E+06	97.01	10430.66	88.75	30.30	0.458
	2	6.7	17.43	5.55	8.49E+06	103.09	11085.03	48.36		
	3	7.4	17.21	4.72	5.20E+06	98.73	10615.86	64.30		
	Average		**16.93**	**5.45**	**6.15E+06**	**99.61**	**10710.52**	**67.14**		
B-0.10	1	7.1	15.24	4.97	3.09E+06	94.01	10108.80	108.64	13.15	0.043
	4	6.6	15.73	5.84	3.32E+06	103.95	11177.47	130.93		

Sample name	Sample	Air-Voids	Peak load (kN)	l75(mm)	|m75| (N/m)	W_f (J)	G_f (J/m^2)	CT_{index}	CoV(%)*	*p-value
	Average		**15.49**	**5.41**	**3.21E+06**	**98.98**	**10643.14**	**119.79**		
B-0.15	1	6.7	17.95	4.58	4.97E+06	99.30	10677.29	65.60	22.87	0.188
	2	7.3	16.40	5.01	4.30E+06	114.60	12323.04	95.68		
	3	7.1	21.11	4.41	5.68E+06	118.21	12710.66	65.79		
	Average		**18.49**	**4.67**	**4.98E+06**	**110.70**	**11903.66**	**75.69**		

Table 12. IDEAL-CT Test Results for 5% RAS Asphalt Mixtures Modified With Varying Dosages

Sample name	Sample	Air-Voids	Peak load (kN)	I75(mm)	|m75| (N/m)	W_f (J)	G_f (J/m^2)	CT_{index}	CoV (%)*	*p-value
Control Mix (CM)	1	7.1	20.21	4.36	1.445×10^7	79.80	8580.72	17.24	26.18	N/A
	2	6.7	18.53	3.49	8.34E+06	61.79	6643.69	18.52		
	4	7.2	19.07	3.93	7.96E+06	77.30	8311.69	27.35		
	Average		**19.27**	**3.92**	**8.15E+06**	**72.96**	**7845.37**	**21.04**		
A-0.05	1	6.5	20.24	4.29	9.07E+06	84.86	9125.06	28.78	7.06	0.071
	2	7.1	18.89	4.58	9.09E+06	87.12	9367.78	31.45		
	4	7.2	21.42	4.96	1.103×10^7	102.7	11047.7	33.14		
	Average		**20.18**	**4.61**	**9.08E+06**	**91.58**	**9846.87**	**31.12**		
A-0.1	1	7.5	20.08	5.19	6.38E+06	114.2	12282.1	66.58	33.64	0.079
	3	7.4	18.91	4.05	6.94E+06	78.19	8407.62	32.70		
	4	6.7	18.13	4.83	6.79E+06	114.7	12336.5	58.49		
	Average		**19.04**	**4.69**	**6.71E+06**	**102.3**	**11008.7**	**52.59**		
A-0.15	1	7.1	16.98	4.49	3.99E+06	100.6	10817.8	81.01	32.72	0.004
	2	7.0	18.88	5.86	4.15E+06	132.0	14203.1	133.89		
	4	7.3	20.71	5.01	5.54E+06	118.4	12736.2	76.80		
	Average		**18.85**	**5.12**	**4.56E+06**	**117.0**	**12585.7**	**97.23**		
B-0.05	1	7.0	17.81	4.86	5.59E+06	84.31	9065.61	52.47	4.72	0.004
	2	6.9	17.10	4.47	5.52E+06	92.77	9975.20	53.85		
	4	6.6	17.59	4.27	5.50E+06	88.31	9496.10	49.09		
	Average		**17.50**	**4.53**	**5.54E+06**	**88.46**	**9512.30**	**51.80**		
B-0.10	2	7.0	20.52	4.28	4.95E+06	107.5	11565.0	66.65	25.38	0.04
	3	7.0	20.12	4.50	7.35E+06	92.57	9953.24	40.63		
	4	7.5	19.39	5.10	7.21E+06	97.23	10455.1	49.30		

Sample name	Sample	Air-Voids	Peak load (kN)	I75(mm)	|m75| (N/m)	W_f (J)	G_f (J/m^2)	CT_{index}	CoV (%)*	*p-value
	Average		**20.01**	**4.63**	**6.50E+06**	**99.12**	**10657.8**	**52.19**		
B-0.15	1	6.7	20.47	4.74	3.77E+06	146.2	15729.4	132.00	24.17	0.024
	3	7.2	18.35	4.49	4.12E+06	102.7	11045.6	80.38		
	4	7.1	16.00	6.14	4.04E+06	99.37	10685.1	108.33		
	Average		**18.27**	**5.13**	**3.97E+06**	**116.1**	**12486.7**	**106.90**		

5. Analysis and Discussion

This section presents the results of the Hamburg Wheel Tracking and Cracking Tolerance Index tests conducted in this study. Graphical plots were developed to illustrate the observed trends in rutting and cracking performance. Formal statistical comparisons were subsequently conducted using one-way ANOVA and post hoc tests, as described in the following sections.

5.1 Hamburg Wheel Tracker Results

5.1.1 HMA With 3% RAS

Figure 14 presents the average rut depth measured after 15,000 wheel passes from the Hamburg Wheel Tracking test for the 3% RAS mix.

Figure 14. Effect of Fiber Type and Content on Rut Depth for HMA with 3% RAS (error bars represent Standard Deviation)

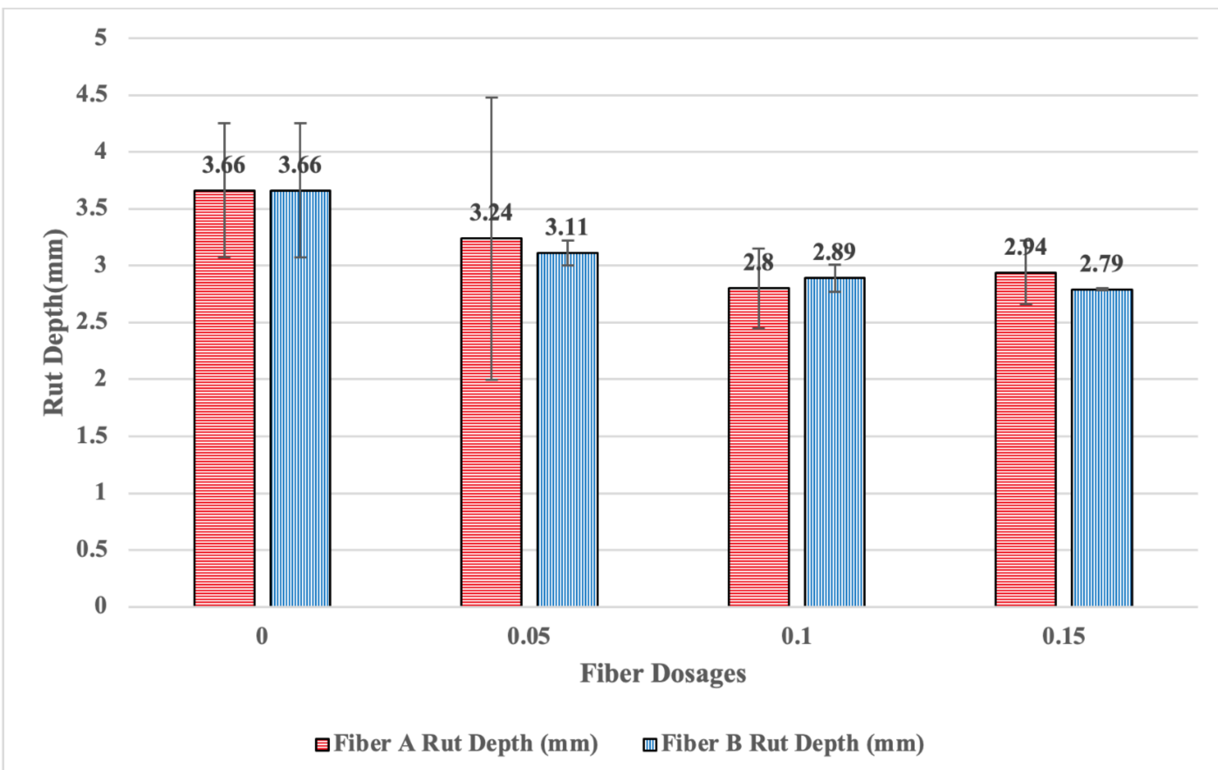

The control mix exhibited the highest rut depth (3.66 mm), indicating the lowest resistance to rutting among the evaluated mixtures. The addition of fibers reduced rut depth for both fiber types across all dosages. At a fiber content of 0.05%, Fiber Type A reduced rut depth to 3.24 mm, while Fiber Type B achieved a slightly lower rut depth of 3.11 mm. This trend suggests that even low fiber dosages contributed to improved rutting resistance compared to the control mix.

As fiber dosage increased, rut depth generally decreased for both fiber types, with the lowest values observed at a fiber content of 0.10%. At this dosage, Fiber Type A and Fiber Type B resulted in rut depths of 2.80 mm and 2.89 mm, respectively. Increasing the fiber content further to 0.15% led to a slight increase in rut depth for Fiber Type A, whereas Fiber Type B continued to show a reduction, achieving the lowest rut depth of 2.79 mm.

Overall, Fiber Type B consistently performed as well as or better than Fiber Type A at equivalent dosages, suggesting that Fiber Type B is more effective in enhancing rutting resistance for the 25% RAP mixture with 3% RAS. These results indicate that an optimal fiber dosage exists near 0.10% to 0.15%, beyond which additional improvements in rutting resistance are limited.

Figure 15 presents the effect of fiber type and fiber content on the stripping inflection point for mixtures containing 3% RAS and 25% RAP. The Stripping Inflection Point (SIP) obtained from the HWT test represents the onset of moisture-induced stripping, identified by a change in slope of the rut depth curve. Aschenbrener (1995) reported that pavements exhibiting good field performance generally had SIP values greater than 10,000 passes, whereas lower SIP values were associated with moisture susceptibility. Based on this guideline, the absence of stripping prior to 10,000 passes is commonly interpreted as satisfactory resistance to moisture damage.

In the present study, no mixture exhibited stripping before 10,000 passes. All evaluated mixes demonstrated SIP values exceeding this threshold, indicating adequate resistance to moisture-induced damage under the tested conditions. Among the evaluated fiber dosages, Fiber B at 0.10% showed the highest SIP, followed by Fiber A at 0.15%, indicating improved stripping resistance with fiber incorporation.

Figure 15. Effect of Fiber Type and Content on Inflection Point for Mixes with 3% RAS

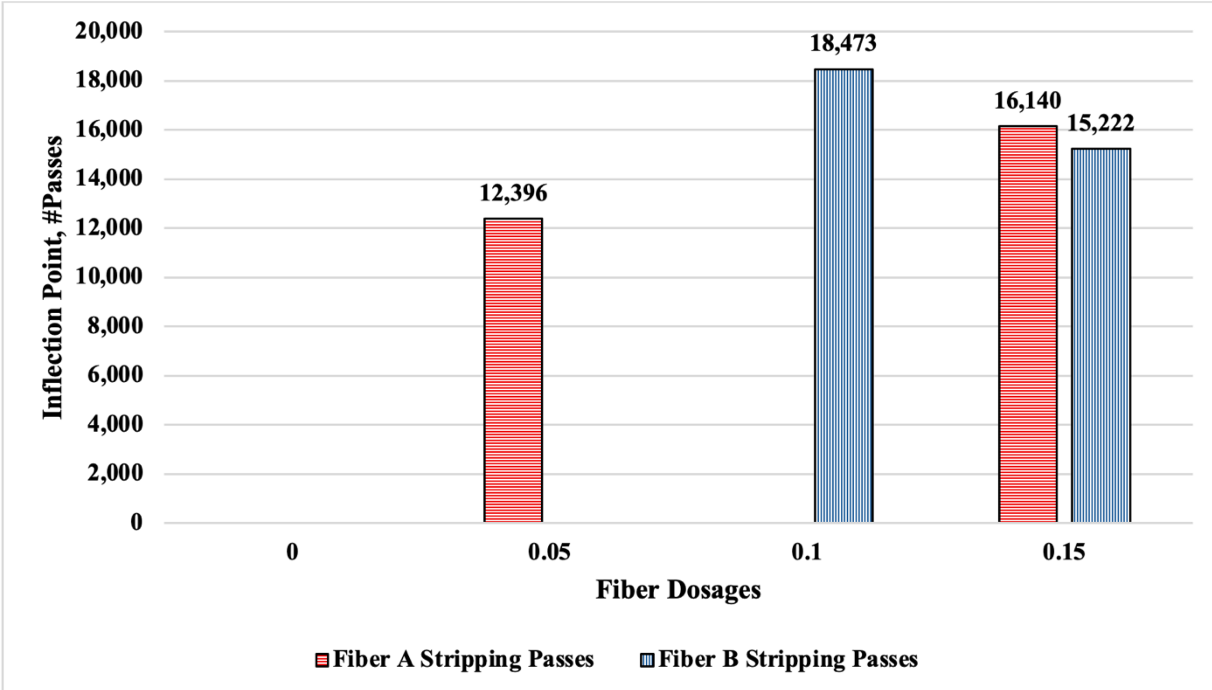

5.1.2 HMA With 5% RAS

Figure 16 presents the effect of fiber type and fiber content on rut depth for HMA mixtures containing 5% RAS and 25% RAP. The control mix exhibited a rut depth of 2.87 mm at 15,000 wheel passes, indicating greater rutting resistance compared to the corresponding 3% RAS mixtures. The addition of fibers further reduced rut depth for both fiber types across all dosages, demonstrating the beneficial role of fiber reinforcement in controlling permanent deformation in mixtures with higher RAS content. For Fiber Type A, rut depth decreased from 2.87 mm for the control mix to values ranging between 2.56 mm and 2.41 mm as fiber content increased.

Figure 16. Effect of Fiber Type and Content on Rut Depth for HMA with 5% RAS
(error bars represent Standard Deviation)

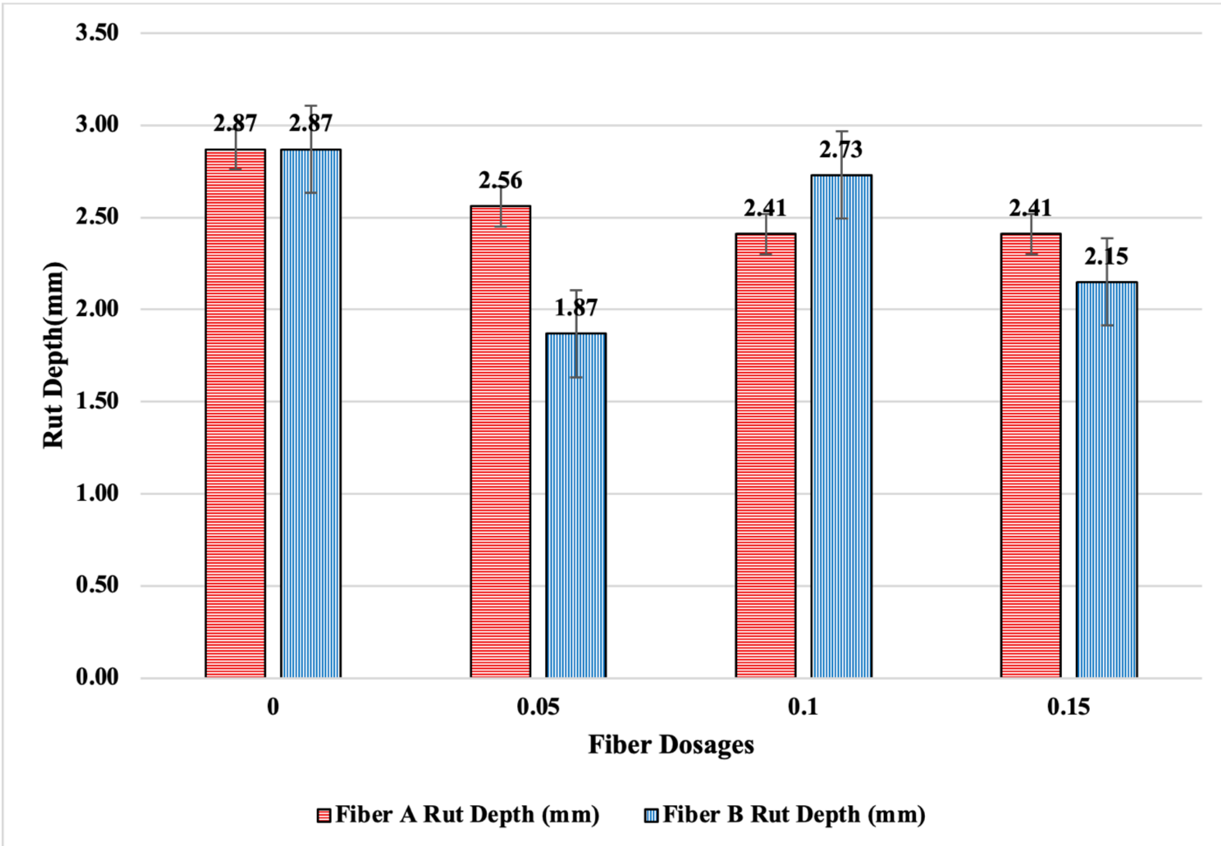

Fiber Type B exhibited a more pronounced improvement in rutting resistance, particularly at lower fiber dosages. At a fiber content of 0.05%, Fiber Type B achieved the lowest rut depth of 1.87 mm, representing the most significant reduction among all evaluated mixtures. Although rut depth increased slightly at a fiber content of 0.10%, Fiber Type B continued to outperform Fiber Type A at equivalent dosages. At 0.15% fiber content, Fiber Type B again demonstrated improved rutting resistance with a rut depth of 2.15 mm. Overall, these results suggest that Fiber Type B is more effective than Fiber Type A in enhancing rutting resistance for 5% RAS mixtures, with optimal performance observed at lower fiber dosages.

Figure 17 shows the effect of fiber type and fiber content on the stripping inflection point for mixtures containing 5% RAS and 25% RAP. Consistent with the interpretation framework discussed previously, the absence of stripping prior to 10,000 passes is considered indicative of acceptable resistance to moisture-induced damage.

For the 5% RAS mixtures evaluated in this study, no stripping was observed before 10,000 passes. All mixtures exhibited SIP values greater than this threshold, indicating adequate resistance to moisture damage under the applied test conditions. While variations in SIP magnitude were observed among fiber types and dosages, the overall performance suggests that increasing RAS content to 5% did not result in premature stripping within the evaluated range.

Figure 17. Effect of Fiber Type and Content on Inflection Point for Mixes with 5% RAS

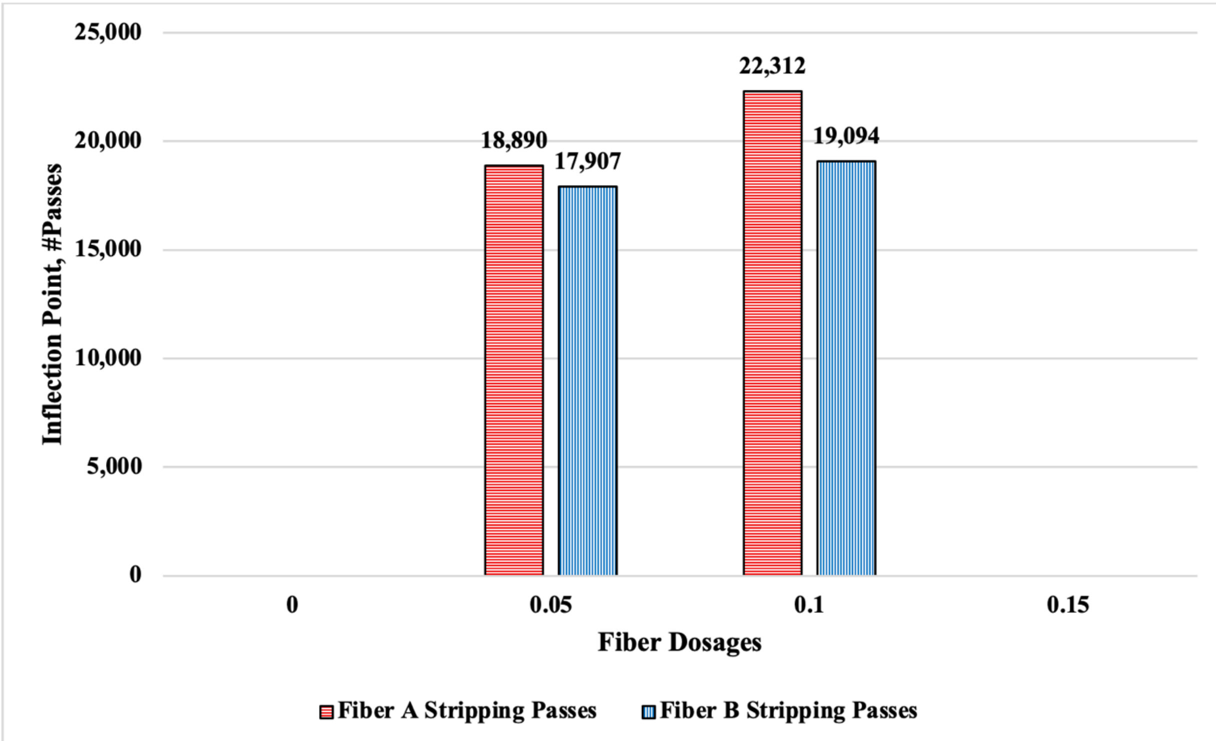

5.1.3 Comparison of All Mixes

Figure 18 presents the average rut depth across all mix combinations with different RAS contents and fiber dosages.

For the control mix, increasing RAS content from 3% to 5% resulted in a noticeable reduction in rut depth, indicating improved rutting resistance with higher RAS content. In general, mixtures containing Fiber Type B exhibited better resistance to rutting compared to those containing Fiber Type A across most fiber dosages and RAS levels.

For the 3% RAS mixtures, both fiber types improved rutting resistance relative to the control mix, with the most notable reductions observed at fiber contents between 0.10% and 0.15%. Fiber Type B at 0.15% showed the lowest rut depth among the 3% RAS mixtures, followed closely by Fiber Type A at 0.10%.

For the 5% RAS mixtures, the effect of fiber addition was more pronounced. Fiber Type B reduced rut depth at all fiber contents compared to the control mix except for 0.10%, with the greatest improvement observed at a fiber content of 0.05%. Fiber Type A also reduced rut depth for the

5% RAS mixtures, although the magnitude of improvement was smaller and more consistent across fiber dosages.

Overall, the results indicate that Fiber Type B is more effective than Fiber Type A in enhancing rutting resistance for 25% RAP mixtures, particularly at higher RAS contents. These findings suggest that the combined use of RAS and Fiber Type B can improve rutting performance and support the use of higher recycled material contents in asphalt mixtures without compromising rutting resistance under HWT conditions.

Figure 18. Average Rut Depth vs. Fiber Content for Mixes with Different RAS Contents

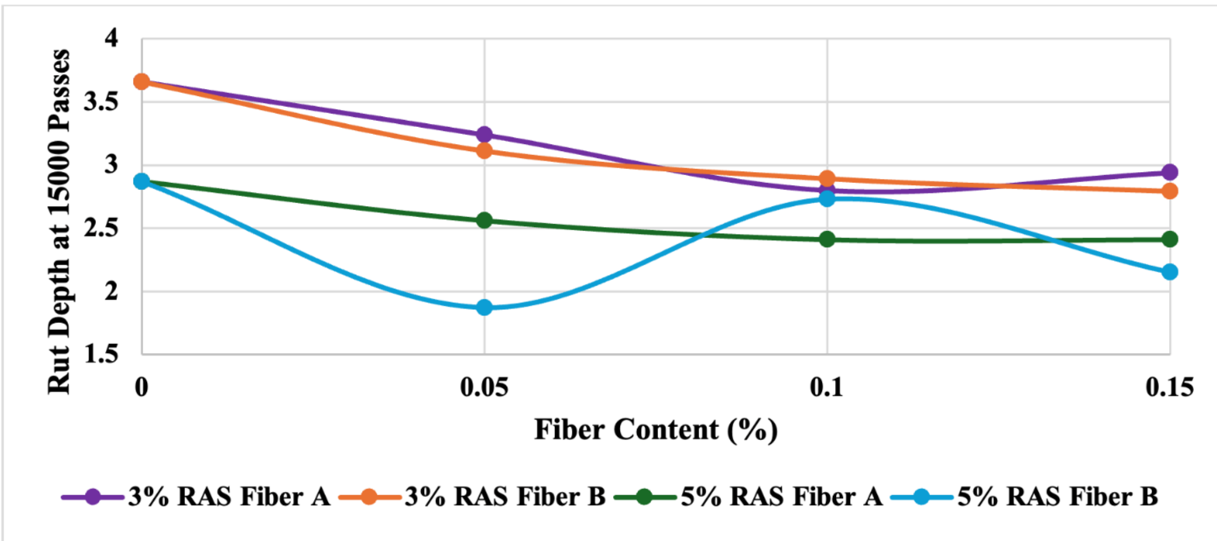

5.1.4 Statistical Analysis

A one-way Analysis of Variance (ANOVA) with Tukey multiple comparison adjustment was performed to evaluate the effects of fiber type and fiber dosage on mixture performance. The response variables investigated were rut depth at 15,000 passes and number of passes at the inflection point.

To compare Fiber A versus Fiber B, the rut depth results from the 3% and 5% RAS mixes were combined and grouped by fiber type (excluding the control mixes). The mean rut depth at 15,000 passes for Fiber B was slightly lower than Fiber A. However, the difference was not statistically significant at the 95% confidence level.

To compare Fiber A and Fiber B, the rut depth results from the 3% and 5% RAS mixtures were combined and grouped by fiber type, excluding the control mixtures. Fiber B had a slightly lower mean rut depth at 15,000 passes than Fiber A, with mean values of 2.59 mm and 2.72 mm, respectively. However, this difference was not statistically significant, $t = 0.65$, $p = 0.5193$.

5.1.5 Inflection Point for Fiber A vs. Fiber B

For the inflection point comparison, the available inflection point results from both RAS levels were combined and grouped by fiber type (excluding the control mixes). Fiber A showed a higher mean number of passes at the inflection point compared to Fiber B (Table 5.3), but the difference was not statistically significant at the 95% confidence level (Table 5.4).

For the inflection point comparison, the available results from both RAS levels were also combined and grouped by fiber type, excluding the control mixtures. Fiber A had a higher mean number of passes at the inflection point than Fiber B, with mean values of 18,973 and 16,577 passes, respectively. However, this difference was not statistically significant, $t = 1.24$, $p = 0.2319$.

5.1.6 Mixes With 3% RAS

Within the 3% RAS group, rut depth results were evaluated separately for Fiber A and Fiber B dosages relative to the control mix. Table 13 shows the mean rut depths at 15,000 passes for the control and Fiber A dosages. Table 14 summarizes the differences in means and Tukey adjusted comparisons versus the control. None of the Fiber A dosages were statistically different from the control at the 95% confidence level. For the 3% RAS HWT rut depth results, a one-way ANOVA was conducted to compare the control mixture and Fiber A mixtures at 0.05%, 0.10%, and 0.15% dosage. The omnibus ANOVA showed no statistically significant effect of Fiber A dosage on rut depth, $F(3, 4) = 0.572$, $p = .663$. For the 3% RAS HWT rut depth results, a one-way ANOVA was also conducted to compare the control mixture and Fiber B mixtures at 0.05%, 0.10%, and 0.15% dosage. The omnibus ANOVA showed no statistically significant effect of Fiber B dosage on rut depth, $F(3, 4) = 3.252$, $p = .142$. Therefore, any differences among the fiber mixtures and the control are interpreted descriptively rather than as statistically significant effects.

Table 13. Mean Rut Depth at 15,000 Passes for the Fiber A Groups (3% RAS)

Group	**Mean Rut Depth at 15,000 passes (mm)**
Control	3.67
0.05% Fiber A	3.24
0.10% Fiber A	2.79
0.15% Fiber A	2.94

Table 14. Tukey Pairwise Comparison for Fiber A Groups (3% RAS)

Group Comparison to Control	Difference in Means (mm)	SE of Difference (mm)	*t*	Adjusted *p*-value	Significance at 95%	95% Confidence Interval
0.05% A - Control	-0.43	0.72	-0.6	.9278	No	(-3.36, 2.50)
0.10% A - Control	-0.87	0.72	-1.21	.6536	No	(-3.80, 2.06)
0.15% A - Control	-0.73	0.72	-1.01	.7515	No	(-3.66, 2.20)

Table 15 shows mean rut depths for the Fiber B dosages and control, while Table 16 presents the Tukey adjusted comparisons versus the control. None of the Fiber B dosages were statistically significant at the 95% confidence level.

Table 15. Mean Rut Depth at 15,000 Passes for the Fiber B Groups (3% RAS)

Group	Mean Rut Depth at 15,000 passes (mm)
Control	3.67
0.05% Fiber B	3.11
0.10% Fiber B	2.9
0.15% Fiber B	2.79

Table 16. Differences in Mean Rut Depth at 15,000 Passes and Confidence Intervals for Fiber B Groups (3% RAS)

Group Comparison	Difference in Means (mm)	SE of Difference (mm)	*t*	Adjusted *p*-value	Significance at 95%	95% Confidence Interval
0.05% B - Control	-0.56	0.3	-1.82	.3821	No	(-1.80, 0.69)
0.10% B - Control	-0.77	0.3	-2.53	.1939	No	(-2.01, 0.47)
0.15% B - Control	-0.87	0.3	-2.85	.1424	No	(-2.11, 0.37)

Inflection point values for the 3% RAS control mixes were not available (NA) in the provided dataset. As a result, statistical comparisons of fiber dosages versus the control for inflection point within the 3% RAS group could not be performed.

5.1.7 Mixes With 5% RAS

Table 17 presents the mean rut depths for the Fiber A groups, and Table 18 provides Tukey adjusted comparisons of the corresponding 5% RAS mixes compared to the control. The 0.10% and 0.15% Fiber A mixes produced statistically significant reductions in rut depth compared to the control mix. For the 5% RAS HWT rut depth results, a one-way ANOVA was conducted to compare the control mixture and Fiber A mixtures at 0.05%, 0.10%, and 0.15% dosage. The omnibus ANOVA showed a statistically significant effect of Fiber A dosage on rut depth, $F(3, 4) = 10.749$, $p = .022$. For the 5% RAS HWT rut depth results, a one-way ANOVA was conducted to compare the control mixture and Fiber B mixtures at 0.05%, 0.10%, and 0.15% dosage. The omnibus ANOVA showed a statistically significant effect of Fiber B dosage on rut depth, $F(3, 4) = 17.979$, $p = .009$.

Table 17. Mean Rut Depth at 15,000 Passes for Fiber A Groups (5% RAS)

Group	**Mean Rut Depth at 15,000 passes (mm)**
Control	2.87
0.05% Fiber A	2.56
0.10% Fiber A	2.41
0.15% Fiber A	2.41

Table 18. Differences in Mean Rut Depth at 15,000 Passes and Confidence Intervals for Fiber A Groups (5% RAS)

Group Comparison	**Difference in Means (mm)**	**SE of Difference (mm)**	***t***	**Adjusted *p*-value**	**Significance at 95%**	**95% Confidence Interval**
0.05% A - Control	-0.31	0.09	-3.31	.0939	No	(-0.69, 0.07)
0.10% A - Control	-0.46	0.09	-4.92	.0267	Yes	(-0.84, -0.08)
0.15% A - Control	-0.46	0.09	-4.92	.0267	Yes	(-0.84, -0.08)

Table 19 presents the mean rut depths for the Fiber B groups, and Table 20 provides Tukey adjusted comparisons of the corresponding 5% RAS mixes compared to the control. The 0.05% and 0.15% Fiber B dosages produced statistically significant reductions in rut depth compared to the control mix.

Table 19. Mean Rut Depth at 15,000 Passes for Fiber B Groups (5% RAS)

Group	**Mean Rut Depth at 15,000 passes (mm)**
Control	2.87
0.05% Fiber B	1.87
0.10% Fiber B	2.73
0.15% Fiber B	2.15

Table 20. Differences in Mean Rut Depth at 15,000 Passes and Confidence Intervals for Fiber B Groups (5% RAS)

Group Comparison	Difference in Means (mm)	SE of Difference (mm)	*t*	Adjusted *p*-value	Significance at 95%	95% Confidence Interval
0.05% B - Control	-1	0.16	-6.32	.011	Yes	(-1.64, -0.35)
0.10% B - Control	-0.14	0.16	-0.86	.8264	No	(-0.78, 0.51)
0.15% B - Control	-0.71	0.16	-4.54	.0349	Yes	(-1.36, -0.07)

Similar to the 3% RAS groups, inflection point values for the 5% RAS control mixes were not available (NA) in the results. As a result, statistical comparisons of fiber dosages versus the control for inflection point within the 5% RAS group could not be performed.

5.2 Cracking Tolerance Index Results

5.2.1 Mixtures With 3% RAS

Figure 19 presents the average CTindex values for asphalt mixtures containing 25% RAP and 3% RAS with varying fiber types and dosages. The control mixture exhibited an average CTindex of 55.42, which represents the baseline cracking resistance for the unmodified 3% RAS mixture.

For mixtures modified with Fiber A, the results show a clear dosage-dependent trend. At a dosage of 0.05%, the CTindex decreased to 41.47, indicating reduced cracking resistance relative to the control mixture. A similar response was observed at 0.10% Fiber A, which produced a CTindex of 42.34. These results suggest that low to moderate dosages of Fiber A did not provide sufficient reinforcement to offset the stiffness introduced by RAS. The fracture response at these dosages indicates limited improvement in post-peak energy dissipation.

When Fiber A content was increased to 0.15%, the CTindex increased to 66.78. This value exceeds the control mixture and suggests improved fracture tolerance at the higher dosage. The increase in CTindex at 0.15% indicates that a greater fiber concentration was required to meaningfully influence crack resistance in mixtures containing 3% RAS. The improvement at this dosage suggests enhanced crack-bridging capability and improved post-peak deformation capacity.

Figure 19. IDEAL-CT Test Results for 3% RAS Asphalt Mixtures Modified with Varying Fiber Types and Dosages (error bars represent Standard Deviation)

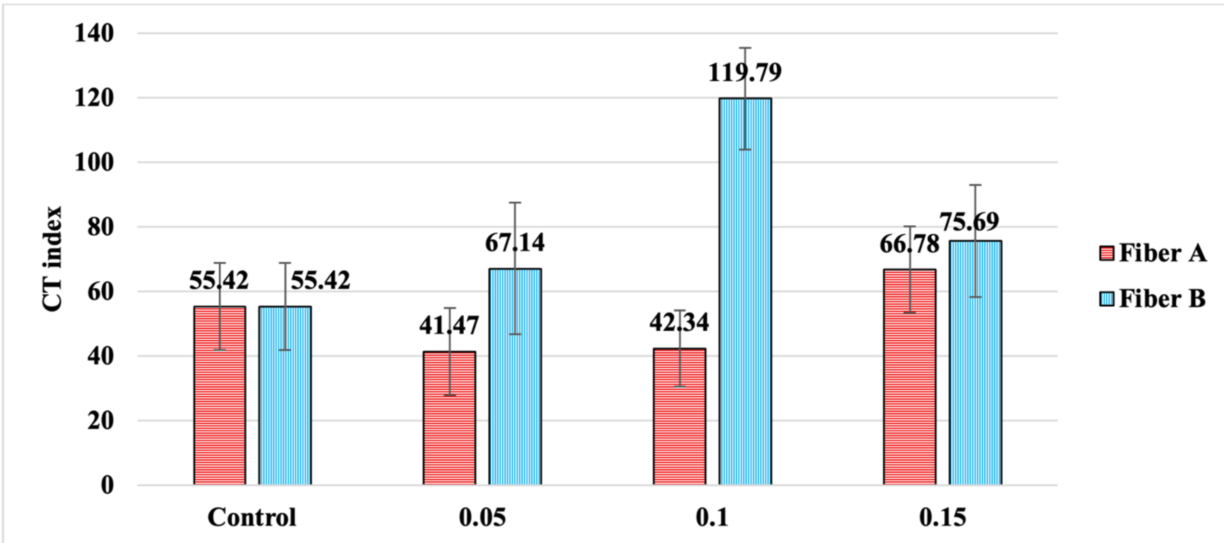

In contrast, mixtures modified with Fiber B exhibited stronger overall performance. At a dosage of 0.05%, Fiber B produced a CTindex of 67.14, which exceeded the control mixture and indicated improved cracking resistance even at relatively low fiber content. This response suggests that Fiber B was more effective at reinforcing the asphalt matrix and promoting ductile fracture behavior.

The most significant improvement was observed at 0.10% Fiber B, where the CTindex reached 119.79. This value represents more than double the control mixture and indicates a substantial enhancement in cracking tolerance. The magnitude of this increase suggests that Fiber B at 0.10% provided an optimal balance between stiffness and ductility, allowing the mixture to sustain greater deformation before failure.

At 0.15% Fiber B, the CTindex decreased to 75.69 compared to the 0.10% dosage, although it remained higher than the control mixture. This reduction suggests that increasing fiber content beyond a certain level did not further enhance fracture performance and may have introduced variability in fiber dispersion or stress distribution within the mixture.

Figure 20 shows the average load–displacement responses for the control mixture and Fiber A-modified mixtures containing 25% RAP and 3% RAS. The control mixture exhibits a relatively sharp post-peak load reduction, indicating brittle fracture behavior and limited deformation capacity after peak load.

At 0.05% Fiber A, the peak load is slightly higher than the control mixture; however, the post-peak response declines rapidly and the curve shortens compared to the control. This behavior is consistent with the lower CTindex value observed for this dosage, indicating that the small amount of fiber was not sufficient to improve fracture resistance.

The 0.10% Fiber A mixture shows a modest increase in peak load and a slightly more gradual post-peak decline compared to the 0.05% mixture. However, the overall post-peak tail remains limited, and the deformation capacity does not significantly exceed that of the control mixture. This corresponds with the CTindex value, which remains below the control average.

At 0.15% Fiber A, the load–displacement curve extends further along the displacement axis and maintains load for a longer duration after peak. Although the peak load is comparable to the other Fiber A mixtures, the longer post-peak tail indicates improved energy dissipation and fracture tolerance. This behavior aligns with the increase in CTindex at 0.15%, suggesting that higher Fiber A content enhances crack-bridging capacity and improves ductility for the 3% RAS mixture.

Overall, Fiber A demonstrates a dosage-dependent effect. Low and moderate dosages do not significantly improve fracture behavior, while the highest dosage produces a noticeable extension in post-peak deformation and improved cracking tolerance.

Figure 20. Comparison of 3% RAS Mixes Containing Fiber A vs. Control Mix (CM)

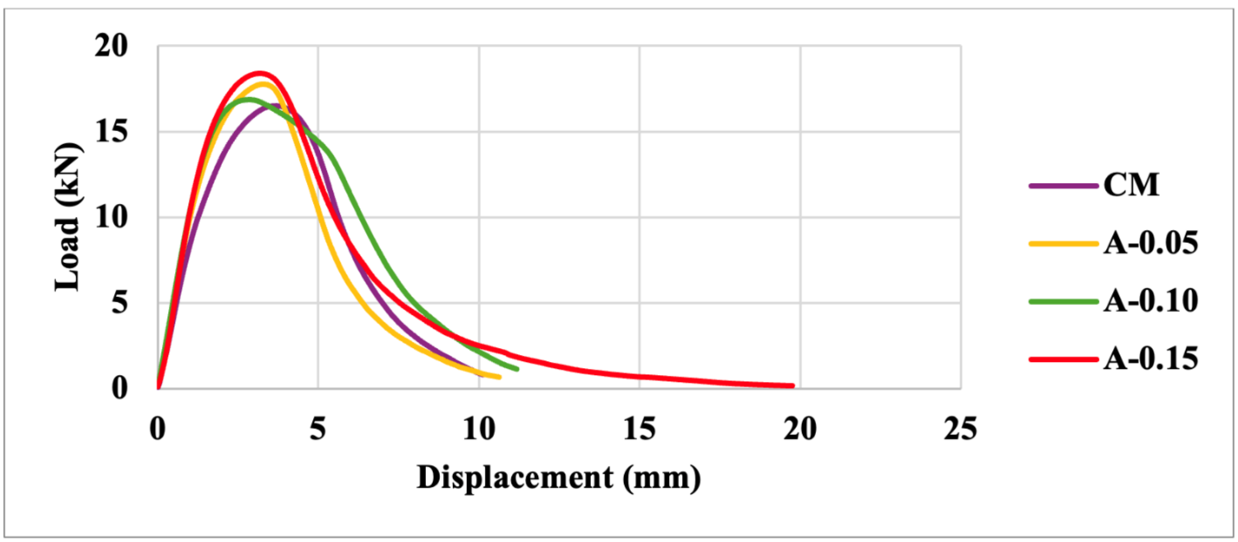

Figure 21 presents the average load–displacement curves for the control mixture and Fiber B-modified mixtures containing 3% RAS. Again, the control mixture shows a steep post-peak decline and limited displacement capacity, consistent with brittle fracture.

At 0.05% Fiber B, the peak load is comparable to the control mixture, but the post-peak region extends further, indicating improved ductility. The curve maintains load over a longer displacement range compared to the control, which is reflected in the higher CTindex value for this mixture. The 0.10% Fiber B mixture shows the most significant change in fracture behavior.

Although the peak load is slightly lower than the control, the post-peak tail is considerably longer and more gradual. The mixture continues to carry load at large displacements, indicating enhanced crack resistance and energy absorption. This extended post-peak behavior explains the substantial increase in CTindex observed for this dosage.

At 0.15% Fiber B, the peak load increases relative to the 0.10% mixture, and the post-peak region remains extended. However, the tail is not as pronounced as the 0.10% mixture in terms of sustained gradual load reduction. The deformation capacity remains higher than the control, but the improvement is less dramatic than that observed at 0.10%.

Overall, the load–displacement behavior suggests that Fiber B is more effective than Fiber A in enhancing cracking resistance for 3% RAS mixtures. The most favorable fracture response is observed at 0.10% Fiber B, where the mixture exhibits sustained post-peak load carrying capacity and improved ductility.

Figure 21. Comparison of 3% RAS Mixes Containing Fiber B vs. Control Mix (CM)

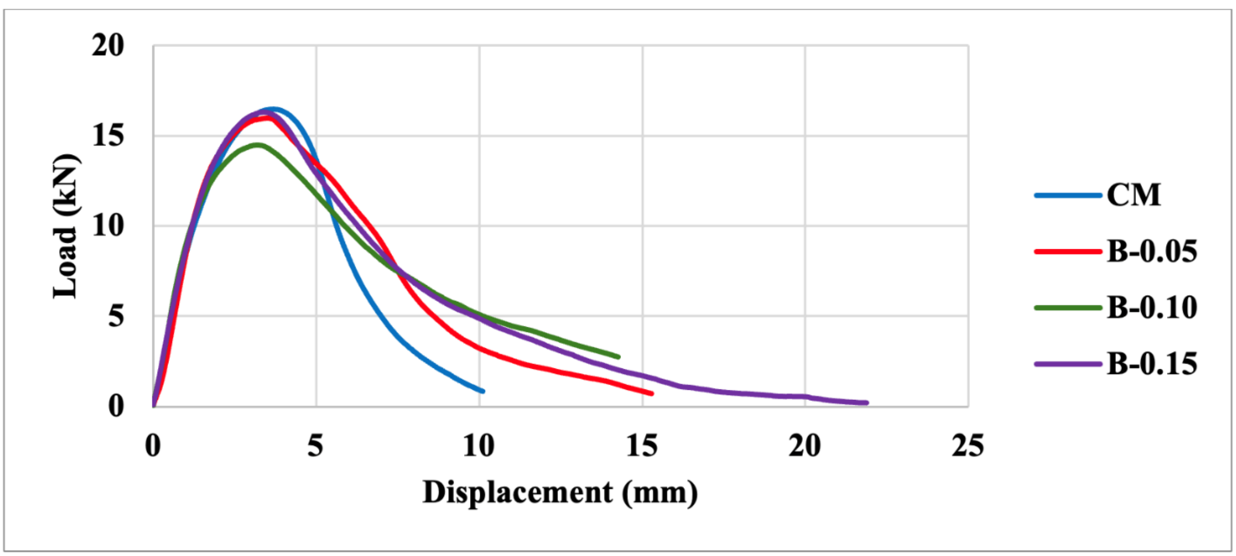

5.2.2 Mixtures With 5% RAS

Figure 22 presents the IDEAL-CT cracking performance of asphalt mixtures containing 25% RAP and 5% RAS modified with Fiber A and Fiber B at dosages of 0.05%, 0.10%, and 0.15%. The control mixture without fibers exhibited an average CTindex of 21.04, which is substantially lower than the corresponding 3% RAS control mixture.

Figure 22. IDEAL-CT Test Results for 5% RAS Asphalt Mixtures Modified with Varying Fiber Types and Dosages (error bars represent Standard Deviation)

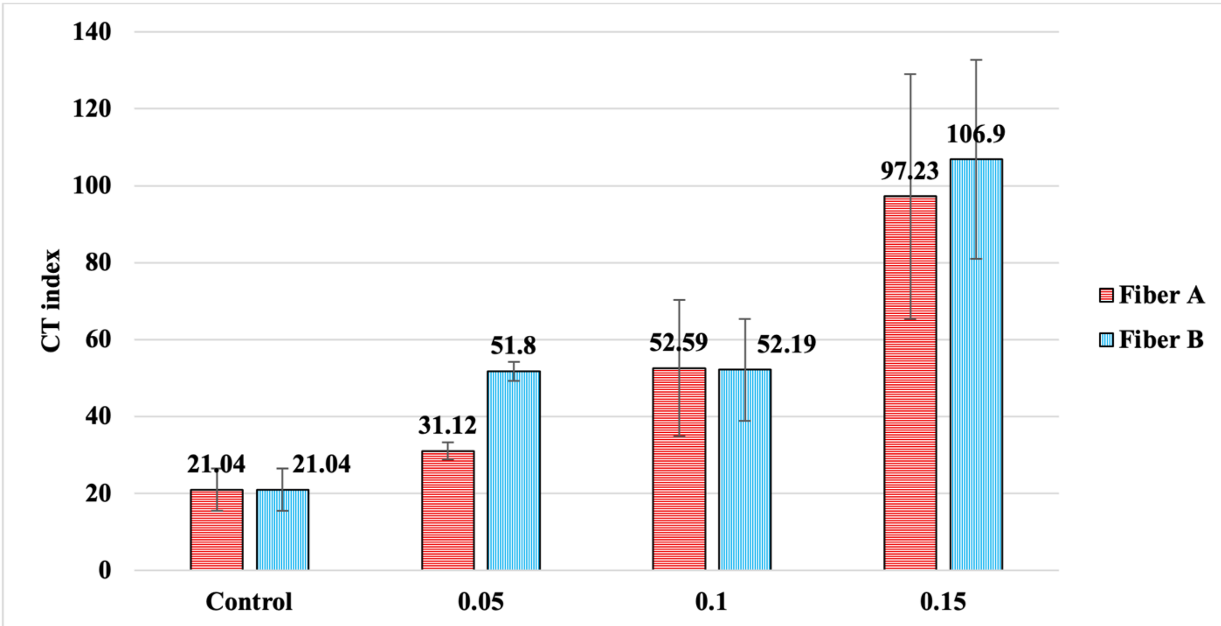

For mixtures modified with Fiber A, a progressive improvement in cracking resistance was observed as fiber dosage increased. At 0.05% Fiber A, the CTindex increased to 31.12, representing a modest improvement over the control mixture. The load–displacement response for this dosage shows slightly greater post-peak deformation compared to the control, although the extension of the tail remains limited.

At 0.10% Fiber A, the CTindex increased to 52.59, indicating a notable improvement in cracking resistance. The load–displacement curve for this mixture demonstrates improved post-peak behavior and sustained load carrying capacity compared to both the control and the 0.05% mixture. The mixture was able to maintain load over a larger displacement range, suggesting improved energy absorption.

The most significant improvement for Fiber A was observed at 0.15%, where the CTindex reached 97.23. This value represents more than four times the control mixture and indicates substantial enhancement in fracture tolerance. The corresponding load–displacement curve shows a pronounced extension of the post-peak region, with the mixture sustaining load at larger displacements.

Mixtures modified with Fiber B also showed strong improvements in cracking resistance compared to the control. At 0.05% Fiber B, the CTindex increased to 51.80, more than double the control value. The load–displacement curve shows a longer and more gradual post-peak decline relative to the control mixture, indicating improved fracture behavior even at low dosage.

At 0.10% Fiber B, the CTindex increased slightly to 52.19, showing performance similar to the 0.05% mixture. The load–displacement behavior indicates improved ductility compared to the control, although the post-peak tail does not extend as far as the higher dosage.

The highest cracking resistance for Fiber B was observed at 0.15%, where the CTindex reached 106.90. This mixture exhibits the most extended post-peak deformation among the Fiber B dosages, indicating strong crack resistance and sustained load carrying capacity at larger displacements.

Overall, the 5% RAS mixtures demonstrate that fiber modification significantly improves cracking resistance compared to the unmodified control. Both fiber types show clear dosage-dependent improvements, with the highest cracking tolerance observed at 0.15% fiber content. Compared to the 3% RAS mixtures, the influence of fiber reinforcement is more pronounced at 5% RAS, where the control mixture exhibits greater brittleness and therefore benefits more substantially from fiber addition.

Figure 23 shows the load–displacement responses for the control mixture and Fiber A–modified mixtures containing 5% RAS. The control mixture exhibits a steep post-peak load reduction and limited displacement capacity, indicating brittle behavior.

At 0.05% Fiber A, the peak load is slightly higher than the control, and the post-peak region extends modestly, suggesting some improvement in cracking resistance. The 0.10% Fiber A mixture shows a more gradual post-peak decline and greater deformation capacity. The most pronounced improvement occurs at 0.15%, where the curve extends significantly farther along the displacement axis and sustains load at larger displacements. This behavior is consistent with the higher CTindex value observed at this dosage.

Overall, Fiber A demonstrates improved fracture performance with increasing dosage, with the strongest response at 0.15%.

Figure 23. Comparison of 5% RAS Mixes Containing Fiber A vs. Control Mix

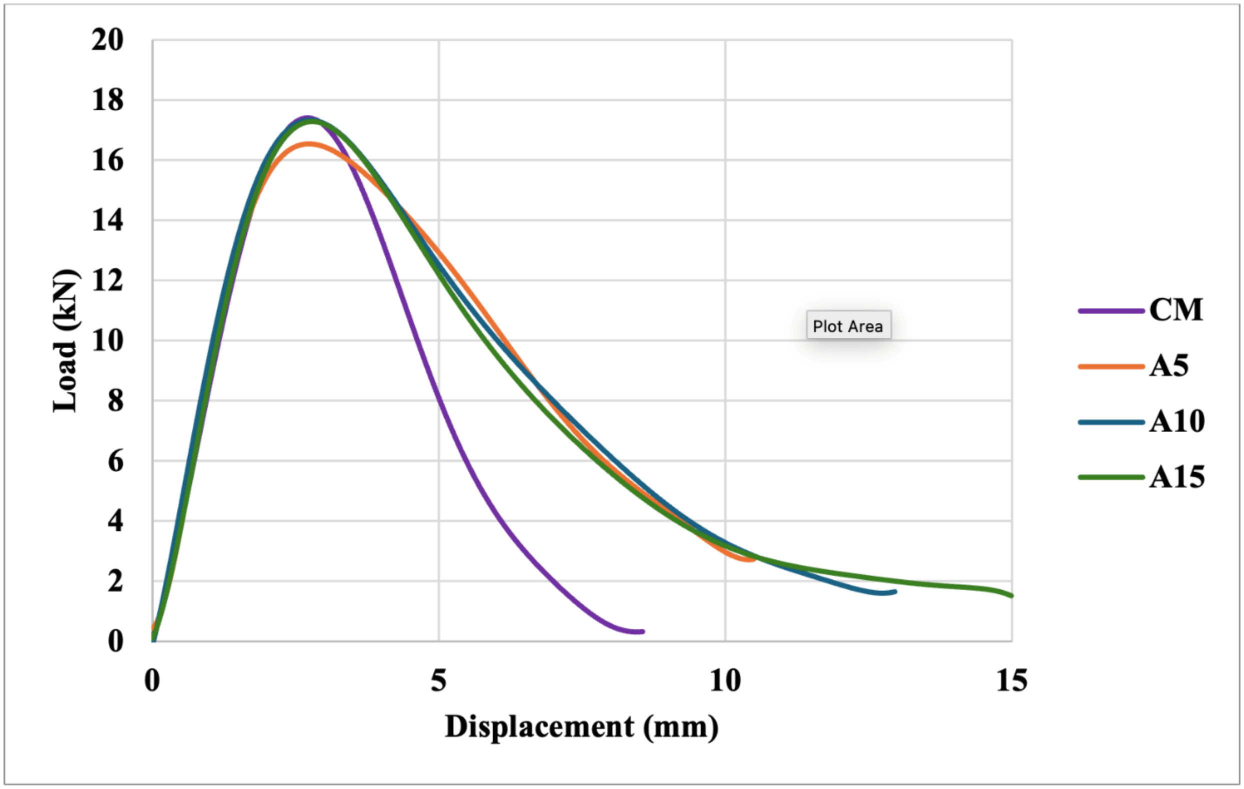

Figure 24 presents the load–displacement curves for Fiber B–modified mixtures. The control mixture again shows rapid load reduction after peak.

At 0.05% Fiber B, the post-peak region extends beyond the control, indicating improved ductility. The 0.10% mixture exhibits the highest peak load and a more gradual post-peak decline. The 0.15% Fiber B mixture shows the longest post-peak tail, sustaining load at larger displacements and demonstrating the greatest fracture tolerance.

Overall, Fiber B improves cracking resistance at all dosages, with the most favorable post-peak behavior observed at 0.15%.

Figure 24. Comparison of 5% RAS Mixes Containing Fiber B vs. Control Mix

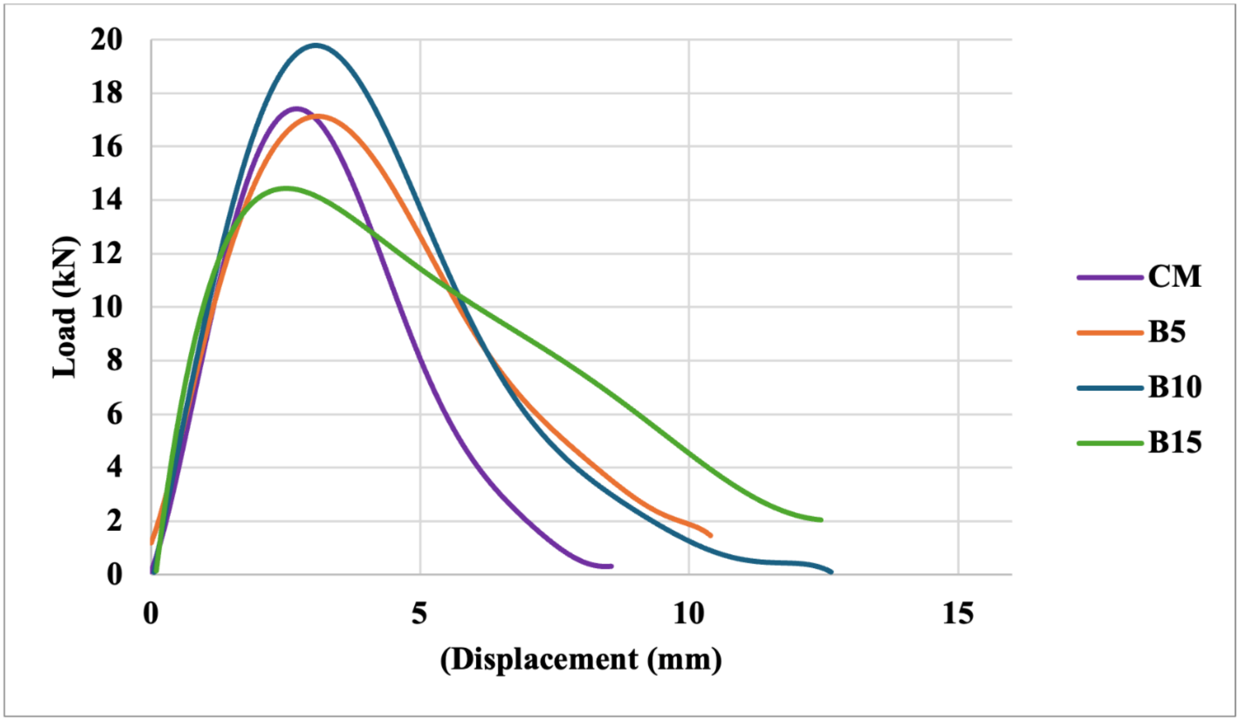

5.2.3 CTI Comparison for All Mix Combinations

Figure 25 presents the IDEAL-CT cracking resistance results for all mixtures containing 3% and 5% RAS. For the control mixtures, increasing RAS content from 3% to 5% resulted in a substantial reduction in CTindex, confirming the increased brittleness associated with higher RAS content. For the 3% RAS mixtures, Fiber B at 0.10% produced the highest CTindex value, followed by 0.15% Fiber B. Fiber A showed improvement only at the highest dosage of 0.15%, while lower dosages of Fiber A resulted in CTindex values below the control mixture.

For the 5% RAS mixtures, fiber modification produced much larger relative improvements compared to the control. Both Fiber A and Fiber B demonstrated increasing cracking resistance with increasing dosage. The highest CTindex values at 5% RAS were observed for 0.15% Fiber B and 0.15% Fiber A, indicating strong improvement in fracture tolerance at higher fiber contents.

Figure 25. CTindex Values of Asphalt Mixtures with 3% and 5% RAS Using Different Fibers and Dosages (error bars represent Standard Deviation)

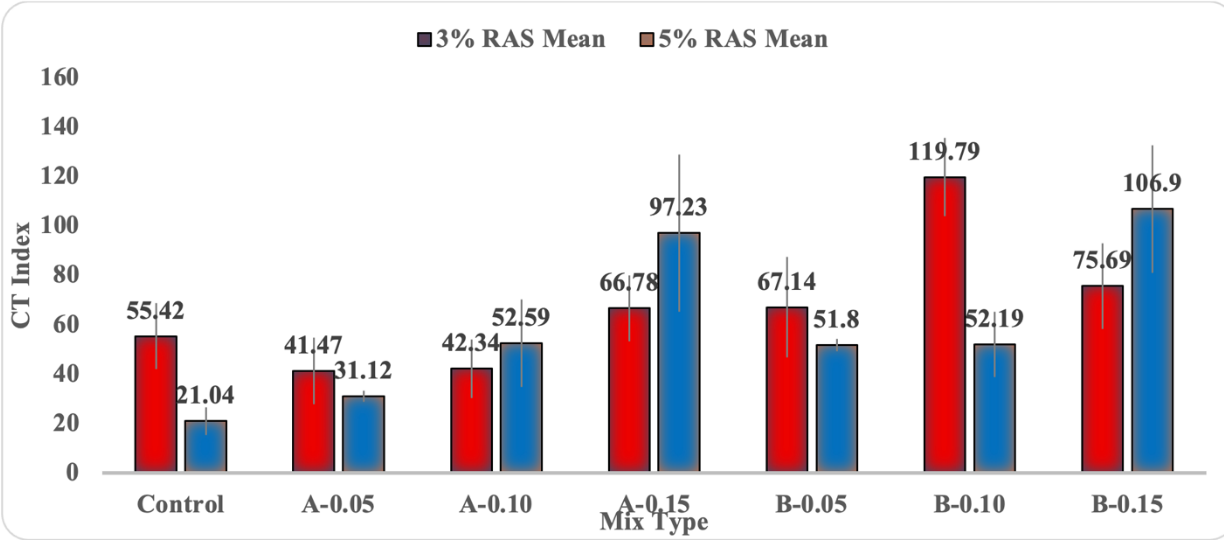

For the 3% RAS CTindex results, a one-way ANOVA was conducted to compare the control mixture and Fiber A mixtures at 0.05%, 0.10%, and 0.15% dosage. The omnibus ANOVA showed no statistically significant effect of Fiber A dosage on CTindex, $F(3, 8) = 2.549$, $p = .129$. Therefore, Fiber A dosage trends at 3% RAS are interpreted descriptively rather than as statistically significant effects. For the 3% RAS CTindex results, a one-way ANOVA was conducted to compare the control mixture and Fiber B mixtures at 0.05%, 0.10%, and 0.15% dosage. The omnibus ANOVA showed a statistically significant effect of Fiber B dosage on CTindex, $F(3, 7) = 6.125$, $p = .023$.

For the 5% RAS CTindex results, a one-way ANOVA was conducted to compare the control mixture and Fiber A mixtures at 0.05%, 0.10%, and 0.15% dosage. The omnibus ANOVA showed a statistically significant effect of Fiber A dosage on CTindex, $F(3, 8) = 10.091$, $p = .004$. For the 5% RAS CTindex results, a one-way ANOVA was conducted to compare the control mixture and Fiber B mixtures at 0.05%, 0.10%, and 0.15% dosage. The omnibus ANOVA showed a statistically significant effect of Fiber B dosage on CTindex, $F(3, 8) = 17.418$, $p < .001$. For each RAS level and fiber type, each fiber dosage was compared against the control group (0% fiber) at the 95% confidence level. Results are summarized in Table 21.

Table 21. Statistical Significance of Each Fiber Mix Compared to the Control Mix

RAS %	Fiber Type	Fiber Percentage	p-value	Significant at p < .05
3%	A	0.05%	0.273	No
3%	A	0.10%	0.275	No
3%	A	0.15%	0.357	No
3%	B	0.05%	0.458	No
3%	B	0.10%	0.043	Yes
3%	B	0.15%	0.188	No
5%	A	0.05%	0.071	No
5%	A	0.10%	0.08	No
5%	A	0.15%	0.004	Yes
5%	B	0.05%	0.0042	Yes
5%	B	0.10%	0.04	Yes
5%	B	0.15%	0.0247	Yes

For the 3% RAS mixtures with Fiber A, none of the fiber dosages produced a statistically significant change in CTindex compared to the control (0.05%: $p = .273$; 0.10%: $p = .275$; 0.15%: $p = .357$). This indicates that under 3% RAS conditions, Fiber A did not produce a statistically reliable improvement in cracking tolerance relative to the control mixture.

For the 3% RAS mixtures with Fiber B, only the 0.10% dosage showed a statistically significant improvement in CTindex compared to the control ($p = .043$). The 0.05% and 0.15% dosages were not statistically different from the control ($p = .458$ and $p = .188$). This suggests that at 3% RAS, Fiber B can improve cracking resistance, but the effect is dosage dependent and only confirmed at the 0.10% dosage.

For the 5% RAS mixtures with Fiber A, the 0.05% and 0.10% dosages were not statistically significant compared to the control ($p = .071$ and $p = .080$). The 0.15% dosage produced a statistically significant improvement relative to the control ($p \approx .004$). This indicates that for mixtures containing 5% RAS, Fiber A required the highest dosage to achieve a reliable improvement in cracking tolerance.

For the 5% RAS mixtures with Fiber B, all dosages produced statistically significant improvements relative to the control: The 0.05%, 0.10%, and 0.15% dosages yielded *p*-values of .0042, .040, and .0247, respectively. This indicates that at 5% RAS, Fiber B improved cracking tolerance consistently, even at the lowest dosage.

Overall, the statistical results show that fiber effectiveness depended on RAS content, fiber type, and dosage. Under 3% RAS, only Fiber B at 0.10% produced a statistically significant improvement. Under 5% RAS, Fiber A showed a statistically significant improvement only at 0.15%, while Fiber B produced statistically significant improvements at all evaluated dosages. These findings support selecting fiber type and dosage based on the specific RAS level rather than applying a single dosage across all mixtures.

6. **Summary and Conclusions**

This study evaluated the performance of hot mix asphalt mixtures containing 25% reclaimed asphalt pavement (RAP), reclaimed asphalt shingles (RAS) at two levels (3% and 5%), and two polymer fiber types at varying dosages. Rutting and moisture resistance were evaluated using the Hamburg Wheel Tracking (HWT) test, and intermediate-temperature cracking resistance was assessed using the IDEAL Cracking Test. The objective was to determine whether polymer fiber reinforcement can offset the brittleness introduced by RAS and support higher recycled material usage within a performance-based design framework. The following conclusions are drawn from this investigation:

Increasing RAS content from 3% to 5% in the control mixtures improved rutting resistance but substantially reduced cracking tolerance, clearly demonstrating the stiffness and brittleness introduced by higher RAS binder replacement.

1. Polymer fiber addition did not compromise rutting resistance; in several cases, rut depth was further reduced compared to the control mixtures, indicating that cracking improvements were achieved without sacrificing deformation resistance.

2. For rutting performance, statistically significant reductions in rut depth were observed in the 5% RAS mixtures for Fiber A at 0.10% and 0.15% and for Fiber B at 0.05% and 0.15%, confirming that fiber modification can meaningfully improve high-temperature performance at elevated RAS contents.

3. Fiber reinforcement effectively restored and enhanced cracking resistance in RAS-modified mixtures, particularly at the higher 5% RAS level where brittleness was most pronounced.

4. For cracking performance, statistically significant improvements in CTindex were observed for Fiber B at 3% RAS and for both fiber types at 5% RAS (with Fiber B significant at all dosages), demonstrating that fiber reinforcement is particularly effective in mitigating cracking susceptibility in high-RAS mixtures.

5. All mixtures exhibited adequate resistance to moisture damage under HWT testing conditions, confirming that increased RAS content and fiber incorporation did not introduce stripping susceptibility.

6. Universal fiber dosage or type is not applicable to all RAS-modified mixtures. Instead, fiber effectiveness is mix-dependent, with higher RAS contents requiring tailored optimization to achieve balanced rutting and cracking performance.

The superior performance of Fiber B compared to Fiber A can be attributed to differences in both effective fiber content and surface treatment. Although both fibers possess similar mechanical properties, Fiber B contains a higher proportion of active para-aramid material, resulting in greater reinforcement at equivalent dosage levels. Additionally, the liquid emulsion treatment of Fiber B likely promotes improved dispersion and bonding within the asphalt mastic compared to the wax-treated Fiber A, which may be more prone to clustering and can contribute to increased stiffness. This distinction is particularly important in high-RAS mixtures, where the binder is already highly aged and brittle. As a result, Fiber B more effectively enhances crack bridging and energy absorption, leading to improved cracking resistance while maintaining rutting performance.

Overall, this study demonstrates that mixtures containing 25% RAP and up to 5% RAS can achieve balanced rutting and cracking performance when properly engineered using polymer fiber reinforcement within a performance-based design framework. Although the laboratory results demonstrate promising improvements in mechanical performance, additional research is needed to validate long-term behavior and practical implementation at production scale. Future work should consider the following:

1. Field validation through construction and monitoring of fiber-reinforced RAS test sections under in-service traffic conditions.
2. Evaluation of long-term aging effects on cracking resistance and fiber performance using extended laboratory aging protocols.
3. Assessment of higher RAS contents to determine practical upper limits when fiber reinforcement is incorporated.
4. Evaluation of plant-scale fiber dosages and dispersion and mixing procedures to ensure consistency in production.
5. Comprehensive life-cycle cost and environmental analyses to evaluate the economic and sustainability implications of fiber-reinforced high-RAS mixtures.

Bibliography

Abdalla, A., Faheem, A. F., & Walters, E. (2022). Life cycle assessment of eco-friendly asphalt pavement involving multi-recycled materials: A comparative study. *Journal of Cleaner Production*, *362*, 132471. https://doi.org/10.1016/j.jclepro.2022.132471

Aguirre, M. A., Hassan, M. M., Shirzad, S., Mohammad, L. N., & Cooper, S. B. (2017). Performance of asphalt rejuvenators in hot-mix asphalt containing recycled asphalt shingles. *Transportation Research Record*, *2633*(1), 108–116. https://doi.org/10.3141/2633-13

Almutairi, H., Qabur, A., & Baaj, H. (2024). Laboratory evaluation of asphalt mixtures reinforced with aramid fibres coated with bituminous oils. *Canadian Journal of Civil Engineering*, *52*(2), 144–154. https://doi.org/10.1139/cjce-2023-0244

American Association of State Highway and Transportation Officials. (2017). *Standard practice for design considerations when using reclaimed asphalt shingles (RAS) in asphalt mixtures* (AASHTO PP 78-17).

American Society for Testing and Materials. (2023). *Standard specification for aramid fiber for asphalt mixtures* (ASTM D8395-23). ASTM International.

Aschenbrener, T. (1995). Evaluation of Hamburg wheel-tracking device to predict moisture damage in hot-mix asphalt. *Transportation Research Record*, *1492*, 193–201.

Bastola, N. R., Souliman, M. I., Tripathi, A., & Pearson, A. (2020). Mechanistic analysis and economic benefits of fiber-reinforced asphalt overlay mixtures. *Journal of Materials and Engineering Structures*, *7*, 83–96.

Bennert, T. (2023). Industry practices for adjusting asphalt mixtures to meet balanced mix design specifications. Presentation Proceedings of the Northeast Asphalt User-Producer Group Annual Meeting.

Blankenship, P., & Simons, M. (2024). *Field performance of aramid fibre reinforced pavements* [Conference paper]. 2024 Transportation Association of Canada Annual Conference, Vancouver, British Columbia, Canada.

California Department of Transportation. (2025). *Senate Bill 1 (SB1)*.

Cao, K., Duan, S., Yu, W., Kang, J., Xu, L., & Sheng, Y. (2025). Performance evaluation and durability assessment of bamboo fiber-reinforced stone mastic asphalt mixtures. *Case Studies in Construction Materials*, *22*, e04790. https://doi.org/10.1016/j.cscm.2025.e04790

Cooper, S. B., Mohammad, L. N., & Elseifi, M. A. (2017). Laboratory performance of asphalt mixtures containing recycled asphalt shingles and re-refined engine oil bottoms. *Journal of Materials in Civil Engineering*, *29*(9), 04017106. https://doi.org/10.1061/(ASCE)MT.1943-5533.0001904

Danislav Drašković and Ljubo Glamočić (2023). Influence of aramid and polyolefin on the technical operational characteristics of asphalt constructions. *Transport and Telecommunication Technology*, *8*(1–2), 5–12. https://doi.org/10.7251/JTTTP2302005D

Federal Highway Administration. (2018). *State of the knowledge for use of asphalt mixtures with reclaimed binder content* (FHWA-HIF-18-059). U.S. Department of Transportation.

Federal Highway Administration. (2021). *Practices and lessons learned when using reclaimed asphalt shingles in asphalt mixtures* (FHWA-HIF-22-001). U.S. Department of Transportation.

Federal Highway Administration. (2022a). *Responsible use of reclaimed asphalt shingles in asphalt mixtures* (FHWA HIF 22-001). U.S. Department of Transportation.

Federal Highway Administration. (2022b). *Balanced asphalt mix design: Eight tasks for implementation* (FHWA HIF 22 048). U.S. Department of Transportation.

Federal Highway Administration. (2024). *Life cycle cost analysis primer* (FHWA HIF 24 0XX). U.S. Department of Transportation.

Ghabchi, R., Zaman, M., Singh, D., Barman, M., & Boeck, D. L. (2021). Effectiveness of using polymer-modified asphalt binders in enhancing fatigue life of asphalt mixes containing RAS and RAP. In M. Barla, A. Di Donna, & D. Sterpi (Eds.), *Challenges and innovations in geomechanics* (pp. 213–219). Springer. https://doi.org/10.1007/978-3-030-64518-2_28

Haas, E., Ericson, C. L., & Bennert, T. (2019). Laboratory-designed hot-mix asphalt mixtures with post-consumer recycled asphalt shingles (RAS) utilizing AASHTO PP78. *Construction and Building Materials*, *226*, 662–672. https://doi.org/10.1016/j.conbuildmat.2019.07.314

Harder, G. A. (2023, September 28). Balanced mix design. *Asphalt Magazine*, *37*(2), 22–27. https://www.asphaltmagazine.com/balanced-mix-design/

Karanam, G. D., & Underwood, B. S. (2024). Mechanical characterization and performance prediction of fiber-modified asphalt mixes. *International Journal of Pavement Research and Technology*, *19*, 134–152. https://doi.org/10.1007/s42947-024-00445-9

Karki, P., Zhou, F., Nyamuhokya, T., Estevanott, M. S., & Mraiza, Z. (2021). *Development of a laboratory testing protocol to evaluate alternative materials for use in modifying asphalt binders and alternative materials for use in modifying asphalt mixtures* (Tech. Rep. BE719). Texas A&M Transportation Institute; Florida Department of Transportation. https://rosap.ntl.bts.gov/view/dot/62348

Khan, A. R., Ali, A., Mehta, Y., & Lein, W. (2024). Laboratory performance characterization of polyolefin/aramid fibers and synthetic aramid fibers reinforced asphalt mixtures. *Construction and Building Materials*, *419*, 135576. https://doi.org/10.1016/j.conbuildmat.2024.135576

Leiva-Villacorta, F., & Julian, G. (2020). *Laboratory and field characterization of warm asphalt mixes with high reclaimed asphalt pavement contents in Alabama* (NCAT Report 20 01). National Center for Asphalt Technology. https://www.eng.auburn.edu/research/centers/ncat/files/technical-reports/rep20-01.pdf

Li, B., Zhou, Y., Wu, Z., Kang, A., Wu, B., & Luo, C. (2023). Influence of basalt fiber on performance of thin overlayer asphalt mixtures based on multiple experimental methods. *Frontiers in Energy Research*, *11*, 1328676. https://doi.org/10.3389/fenrg.2023.1328676

Lin, P., Liu, X., Ren, S., Li, Y., Xu, J., & Li, M. (2023). Unraveling the influence of fibers on aging susceptibility and performance of high content polymer modified asphalt mixtures. *Case Studies in Construction Materials*, *18*, e02211. https://doi.org/10.1016/j.cscm.2023.e02211

Liu, J., Yan, K., Liu, J., & Zhao, X. (2018). Using artificial neural networks to predict the dynamic modulus of asphalt mixtures containing recycled asphalt shingles. *Journal of Materials in Civil Engineering*, *30*(4), 04018051. https://doi.org/10.1061/(ASCE)MT.1943-5533.0002242

Mateos, A., & Harvey, J. (2019). *Laboratory evaluation of the mechanical properties of asphalt concrete reinforced with aramid synthetic fibers* (UCPRC-RR-2019-01). University of California Pavement Research Center. https://escholarship.org/uc/item/40j1p8k7

Mivehchi, M., Wen, H., Wen, Y., & Wang, L. (2023). Study of measures to design asphalt mixes including high percentages of recycled asphalt pavement and recycled asphalt shingles. *Transportation Research Record*, *2677*(2), 869–879. https://doi.org/10.1177/03611981221108982

Mocelin, D. M., Isied, M. M., & Castorena, C. (2023). Influence of reclaimed asphalt pavement and recycled asphalt shingle binder availability on the composition of asphalt mixtures. *Journal of Cleaner Production*, *426*, 139156. https://doi.org/10.1016/j.jclepro.2023.139156

Mogawer, W. S., Austerman, A. J., Bonaquist, R., & Roussel, M. (2011). Performance characteristics of thin-lift overlay mixtures containing high reclaimed asphalt pavement content, recycled asphalt shingles, and warm-mix asphalt technology. *Transportation Research Record*, *2208*(1), 17–25. https://doi.org/10.3141/2208-03

Musa, N. F. A. A., Aman, M. Y., Shahadan, Z., Taher, M. N. M., & Noranai, Z. (2019). Utilization of synthetic reinforced fiber in asphalt concrete – A review. *International Journal of Civil Engineering and Technology*, *10*(5), 678–694. https://iaeme.com/MasterAdmin/Journal_uploads/IJCIET/VOLUME_10_ISSUE_5/IJCIET_10_05_070.pdf

National Asphalt Pavement Association. (2016). *Use of RAP and RAS in high binder replacement asphalt mixtures* (Special Report 213).

National Asphalt Pavement Association. (2019). *Guidelines for the use of reclaimed asphalt shingles in asphalt pavements* (2nd ed., Information Series 136).

National Asphalt Pavement Association. (2024). *The carbon footprint of asphalt pavements: A reference document for decarbonization* (SIP 109).

National Asphalt Pavement Association. (2025). *Balanced mix design resource guide*.

National Center for Asphalt Technology. (2024). *Phase VIII (2021-2024) NCAT Test Track findings: Full report* (24-01). Auburn University Samuel Ginn College of Engineering. https://eng.auburn.edu/research/centers/ncat/files/Phase-8-TT-Full-Report-9-30-24.pdf

Nian, T., Wang, M., Huang, X., Ge, J., Song, J., & Li, P. (2024). Investigating crack resistance and mechanisms of crack extension in high-content steel fibers reinforced hot recycled asphalt mixtures. *Construction and Building Materials*, *450*, 138717. https://doi.org/10.1016/j.conbuildmat.2024.138717

Noorvand, H. (2024, January). *ES04: Recycled materials, additives, and fibers use in asphalt mixtures* [University Presentation]. Pavement Engineering, Arizona State University. https://pavement.engineering.asu.edu/wp-content/uploads/sites/16/2024/01/ES04-Hossein-Noorvand.pdf

Noorvand, H., Noorvand, H., Castro, S., Underwood, B. S., & Kaloush, K. E. (2022). Evaluating interaction of fibre reinforcement mechanism with mesostructure of asphalt concrete. *International Journal of Pavement Engineering*, *23*(5), 1594–1611. https://doi.org/10.1080/10298436.2020.1813286

Northeast Center for Excellence in Pavement Technology. (2024). *Material and structural characterization of fiber reinforced asphalt pavements in Pennsylvania using Forta fiber products: Fibre study report - PA manufacturing* [Technical report]. Pennsylvania State University Larson Transportation Institute. https://www.superpave.psu.edu/assets/docs/Fibe-Study-Report-PA-Manufacturing-Oct-2024.pdf

Obaid, H. A., Eltwati, A., Hainin, M. R., & Tarhuni, F. (2024). Experimental investigation and statistical analysis of performance of ceramic fiber-reinforced warm asphalt mixtures containing reclaimed asphalt pavement. *Construction and Building Materials*, *455*, 139230. https://doi.org/10.1016/j.conbuildmat.2024.139230

Slebi-Acevedo, C. J., Lastra-González, P., Pascual-Muñoz, P., & Castro-Fresno, D. (2019). Mechanical performance of fibers in hot mix asphalt: A review. *Construction and Building Materials*, *200*, 756–769. https://doi.org/10.1016/j.conbuildmat.2018.12.171

Rahim, A., Saadeh, S. M., & Al Zaraiee, H. (2025). *Use of polymer fiber to improve mechanical properties of HMA containing recycled asphalt pavement (RAP)* (Report No. 25-22). Mineta Transportation Institute, San José State University. https://doi.org/10.31979/mti.2025.2462

Rangelov, M., Dylla, H., & Sivaneswaran, N. (2021). Life-cycle assessment of asphalt pavements with recycled post-consumer polyethylene. *Transportation Research Record*, *2675*(12), 443–455. https://doi.org/10.1177/03611981211033862

Riccardi, C., Wang, D., Wistuba, M. P., & Walther, A. (2023). Effects of polyacrylonitrile fibres and high content of RAP on mechanical properties of asphalt mixtures in binder and base layers. *Road Materials and Pavement Design*, *24*(9), 2133–2155. https://doi.org/10.1080/14680629.2022.2117072

San Diego County Department of Public Works. (2025). Reclaimed asphalt shingles (RAS) [Guidance Document S-3].

Serin, S., Önal, Y., Emiroğlu, M., & Demir, E. (2023). Comparison of the effect of basalt and glass fibers on the fracture energy of asphalt mixes using semi-circular bending test. *Construction and Building Materials*, *406*, 133460. https://doi.org/10.1016/j.conbuildmat.2023.133460

Shanbara, H. K., Musa, S. S. and Dulaimi, A. (2020). The effect of polypropylene fibres on the tensile performance of asphalt mixtures for road pavements. *IOP Conference Series: Materials Science and Engineering*, *888*, 012082. https://doi.org/10.1088/1757-899X/888/1/012082

Shirzad, S., Aguirre, M. A., Bonilla, L., Elseifi, M. A., Cooper, S. B., & Mohammad, L. N. (2018). Mechanistic-empirical pavement performance of asphalt mixtures with recycled asphalt shingles. *Construction and Building Materials*, *160*, 687–697. https://doi.org/10.1016/j.conbuildmat.2017.11.114

Sias, J. E. (2024a). *How DOTs can enhance sustainability and resilience in asphalt pavements using RAP and RAS*. National Asphalt Pavement Association, Asphalt Pavement Alliance.

Sias, J. E. (2024b). *How warm-mix asphalt (WMA) supports DOT goals for resilience and sustainability*. National Asphalt Pavement Association.

Slebi-Acevedo, C. J., Lastra-González, P., Calzada-Pérez, M. A., & Castro-Fresno, D. (2020). *Effect of synthetic fibers and hydrated lime in porous asphalt mixture using multi-criteria decision-making techniques*. *Materials*, 13(3), 675. https://doi.org/10.3390/ma13030675

SCS Global Services. (2023). *Environmental product declaration: ACE XP™ polymer fiber*. Surface Tech. https://asphaltepd.org/static/core/upstream_epds/surfacetech/SCS-EPD-09448_SurfaceTech_ACEXP_100423.pdf

Surface Tech. (2024). *LCA analysis: Maximizing value with low carbon asphalt*. https://surface-tech.com/arca-cost/lca/

Surface Tech. (2025). *AQU™ polymer fiber*. https://surface-tech.com/aqu/

Tapkın, S. (2008). The effect of polypropylene fibers on asphalt performance. *Building and Environment*, *43*(6), 1066–1071. https://doi.org/10.1016/j.buildenv.2007.02.011

Williams, B. A., Willis, J. R., & Shacat, J. (2024). *Annual asphalt pavement industry survey on recycled materials and warm-mix asphalt usage: 2022* (Information Series 138). National Asphalt Pavement Association.

Wiśniewski, D., Słowik, M., Kempa, J., Lewandowska, A., & Malinowska, J. (2020). Assessment of impact of aramid fibre addition on the mechanical properties of selected asphalt mixtures. *Materials*, *13*(15), 3302. https://doi.org/10.3390/ma13153302

Wu, S., Zhang, K., Wen, H., DeVol, J., & Kelsey, K. (2016). Performance evaluation of hot mix asphalt containing recycled asphalt shingles in Washington State. *Journal of Materials in Civil Engineering*, *28*(1), 04015088. https://ascelibrary.org/doi/10.1061/%28ASCE%29MT.1943-5533.0001357

Xie, X., He, Y., Liu, C., Wang, K., Fan, Z., Li, H., & Shao, J. (2024). Optimization of the dosage of chopped basalt fibers in asphalt pavement surface course materials for semi-rigid base with functional requirements. *PLoS ONE*, *19*(7), e0307438. https://doi.org/10.1371/journal.pone.0307438

Yan, Y., Hernando, D., Lopp, G., Rilko, W., & Roque, R. (2018). Enhanced mortar approach to characterize the effect of reclaimed asphalt pavement on virgin binder true grade. *Materials and Structures*, *51*, Article 41. https://doi.org/10.1617/s11527-018-1168-1

Zhang, Y., Sang, T., Kang, A., Wang, B., Wu, X., & Zhao, Y. (2023). Investigation of fiber length distribution on crack resistance mechanism of basalt fiber asphalt mixture based on digital image processing technology. *Construction and Building Materials*, *401*, 132753. https://doi.org/10.1016/j.conbuildmat.2023.132753

Zhang, Y., Swiertz, D., & Bahia, H. U. (2021). Use of blended binder tests to estimate performance of mixtures with high reclaimed asphalt pavement/recycled asphalt shingles content. *Transportation Research Record*, *2675*(8), 281–293. https://doi.org/10.1177/0361198121997423

Zhao, H., Guan, B., Xiong, R., & Zhang, A. (2020). Investigation of the performance of basalt fiber reinforced asphalt mixture. *Applied Sciences*, *10*(5), 1561. https://doi.org/10.3390/app10051561

Zhao, H., Li, G., Ma, Y., Yu, X., Chen, Y., & Li, W. (2024). Long-term performance of chemically modified cotton straw fibers in micro-surfacing asphalt mixtures. *Case Studies in Construction Materials*, *20*, e03294. https://doi.org/10.1016/j.cscm.2024.e03294

Zhao, M., Liu, X., Yuan, H., Xu, X., & Wu, K. (2025). Evaluation of asphalt performance for modification using aramid in different forms. *Construction and Building Materials*, *492*, 142901. https://doi.org/10.1016/j.conbuildmat.2025.142901

Zhu, C., Yang, Y., Zhang, K., & Yu, D. (2024). Study on the road performance and compaction characteristics of fiber-reinforced high-RAP plant-mixed hot recycled asphalt mixtures. *Polymers*, *16*(14), 2016. https://doi.org/10.3390/polym16142016

About the Authors

Hani Alzraiee, PhD, PE, PMP

Dr. Alzraiee is an Associate Professor of Construction Engineering at California Polytechnic State University. He has extensive experience in research covering infrastructure asset management, project delivery and contracting, condition assessment of transportation systems, and geospatial technologies.

Ashraf Rahim, PhD, PE

Dr. Rahim is a Professor in the Civil and Environmental Engineering at California Polytechnic State University. He has extensive experience in research dealing with pavement materials characterization, cement treated bases, and the performance of rubberized asphalt.

Shadi M. Saadeh, PhD, PE, M. ASCE

Dr. Saadeh is a Professor of Civil Engineering at the California State University, Long Beach (CSULB). He is also the director of National Center for Transportation, Green Technologies and Education. He has extensive experience in research dealing with pavement materials characterization.

Aaditya Ojha, EIT

Aaditya Ojha is a Graduate Research Assistant in CSULB where he is pursuing an M.S. in Civil Engineering with a transportation focus. He brings over 5 years of field experience in highway construction, underground utilities, and water infrastructure across ADB-funded programs, and he currently supports research on sustainable asphalt mix design, including performance testing of HMA mixtures containing RAP and RAS. He holds a California Engineer in Training (EIT) credential and is an ASCE member.

Adam Mansara

Adam Mansara is a graduate research assistant in Civil Engineering at California Polytechnic State University. He contributed to laboratory testing and data collection for this study, supporting Hamburg Wheel Tracking tests.